

Thermodynamic modeling of melt addition to peridotite: Implications for the refertilization of the non-cratonic continental mantle lithosphere

Pin Juliette ^{1,2,*}, France Lyderic ^{1,3}, Lambart Sarah ⁴, Reisberg Laurie ¹

¹ Université de Lorraine, CNRS, CRPG, F-54000 Nancy, France

² Univ. Brest, CNRS, IUEM, UMR 6538, Laboratoire Géosciences Océan, Place Copernic, 29280 Plouzané, France

³ Institut Universitaire de France (IUF), France

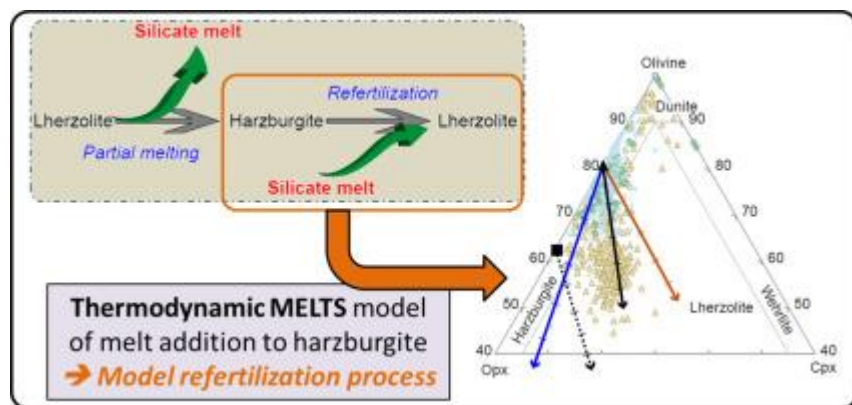
⁴ Department of Geology and Geophysics, University of Utah, Salt Lake City, UT, United States

* Corresponding author : Juliette Pin, email address : juliette.pin@univ-brest.fr

Abstract :

In a classic model of evolution of the non-cratonic continental mantle lithosphere, harzburgites represent the refractory (< 5% clinopyroxene) residues of high degrees of partial melting of fertile mantle, while lherzolites (> 5% clinopyroxene) represent residues of lesser degrees of partial melting. However, partial melting is not the only process that could explain the peridotite compositional variability that ranges from fertile (> 2 wt% Al₂O₃, < 45 wt% MgO) to refractory (< 2 wt% Al₂O₃, > 45 wt% MgO). In the refertilization process, harzburgite is a refractory protolith (potentially previously formed by partial melting of a fertile mantle) that undergoes reactive percolation of silicate melts derived from the underlying asthenosphere, resulting in the crystallization of a new generation of minerals (mostly clinopyroxene). A simple but critical first step towards understanding the refertilization process is to examine how modal and major element compositions evolve as melts are added to peridotites. Here we use a thermodynamically-constrained two-component mixing model to independently evaluate the roles of five different parameters: pressure, temperature, redox conditions, and compositions of the initial peridotite and the added basaltic melt (hereafter referred to P-T-fO₂-X_{pi}-X_{melt}), during melt addition. We compare the results with observed suites of peridotites. The main observations are as follows: (1) the produced model is consistent with the global peridotite database, and (2) T, fO₂ and small variations of pressure have almost no impact on the evolution of the system. In contrast, the mineralogy of the percolated harzburgite has a substantial effect on the variation of the modal proportions. The parameter with the most significant impact is X_{melt}, which is directly linked to the geodynamic context and melting conditions. This parameter directly controls the refertilization reaction and so, the phase proportions and the bulk-rock composition. Elements that partition preferentially in the melt phase (e.g., Na) display depletions in natural assemblages that are stronger than those predicted from the simple mixing model, consistent with the fact that the natural process occurs in an open system, and that reactive percolation likely results in incompatible element enrichment in the associated melt. Our results corroborate the suggestion that most of the spectrum of compositional variability observed in lithospheric mantle peridotites can be explained by the impregnation of primitive silicate melt in refractory harzburgites.

Graphical abstract



Keywords : Continental mantle lithosphere, Refertilization, Mixing model, Peridotites, pHMELTS, Harzburgites, Lherzolites

53 The subcontinental lithospheric mantle (SCLM) is petrologically and geochemically heterogeneous
54 (Allègre & Turcotte, 1986; Hofmann, 1997; Stracke et al., 2005; Griffin et al., 2009; Bodinier &
55 Godard, 2014; Pearson et al., 2014). This lithospheric domain is documented by xenoliths in alkali
56 basalts and kimberlites and by orogenic peridotite massifs. In non-cratonic regions, the SCLM has on
57 average a lherzolitic bulk composition ($> 5\%$ clinopyroxene; Griffin et al., 1999). Lherzolites are
58 fertile peridotites, and are aluminum-rich ($> 2 \text{ wt.}\% \text{ Al}_2\text{O}_3$) and magnesium-poor ($< 45 \text{ wt.}\% \text{ MgO}$).
59 Pyroxenites, dunites and, to a greater extent, harzburgites ($< 5\%$ clinopyroxene) are also common
60 SCLM lithologies. Harzburgites are aluminum-poor ($< 2 \text{ wt.}\% \text{ Al}_2\text{O}_3$) and magnesium-rich (> 45
61 $\text{wt.}\% \text{ MgO}$). The genetic relationships between these rock types have been the subject of much debate
62 in the last decades (e.g., Frey and Prinz, 1978; Kelemen et al., 1992; Le Roux et al., 2007). In addition
63 to potential preexisting compositional variability, the spectrum of natural peridotite compositions can
64 be mostly explained by the combination of two end-member processes (**Fig. 1**): partial melting and
65 refertilization (see reviews by Simon et al., 2008; Bodinier and Godard, 2014; Pearson et al., 2014;
66 Warren, 2016). The partial melting model implies that harzburgites and clinopyroxene-poor
67 lherzolites are formed by variable degrees of partial melting of fertile lherzolites (e.g., Dick et al.,
68 1984; Frey et al., 1985; McKenzie and Bickle, 1988; McKenzie and O'Nions, 1991; Hellebrand et al.,
69 2001). The refertilization model implies that lherzolites are secondary (refertilized) lithologies formed
70 from the interaction between a refractory, lithospheric mantle (mostly harzburgitic) with silicate melts
71 derived from the underlying asthenosphere (e.g., Van der Wal and Bodinier, 1996; Garrido and
72 Bodinier, 1999; Muntener and Piccardo, 2003; Pilet et al, 2005, 2008, 2011) or, more locally, from a
73 secondary melting event of the lithosphere (e.g., Chazot et al., 1996; Rampone et al., 2020). As used
74 in this contribution, the term "refertilization" will refer to the process of modal transformation of
75 harzburgite from the addition of, and/or interaction with silicate melt in the non-cratonic mantle. This
76 can produce clinopyroxene-enriched harzburgite, lherzolite, or other types of peridotite depending on

the percolating melt composition. We do not consider the full range of metasomatic processes and agents that often result in the enrichment of incompatible trace elements and modification of isotopic compositions in peridotites. Nevertheless, we recognize that refertilization and metasomatism represent a continuum of processes and the distinction between them can be ambiguous. We also do not consider processes of metamorphic segregation (e.g., Tilhac et al., 2021) that can contribute to local sharp changes of modal proportions.

Support for the refertilization model is provided by petrographic, geochemical and structural observations. Geochemical evidence comprises variations of trace and major elements in bulk compositions and minerals (e.g., Elthon, 1992; Hellebrand et al., 2002; Le Roux et al., 2007; Soustelle et al., 2009; Mundl et al., 2015; Gu et al., 2016), while structural observations include lherzolite foliations and websterite layering that cross-cut harzburgite deformation (Le Roux et al., 2008). Additionally, the presence of intergranular pyroxenes and spinels, often associated with sulfides (Bodinier & Godard, 2014; Lorand and Luguet, 2016) has been interpreted as secondary phase crystallization from liquid percolation. Al_2O_3 content in the bulk-rock is very frequently used as a proxy for peridotite fertility, though MgO and CaO contents, Yb and Lu concentrations, olivine Fo# ($=\text{MgO}/(\text{MgO}+\text{FeO})\times 100$, in mol.) and spinel Cr# ($=\text{Cr}_2\text{O}_3/(\text{Cr}_2\text{O}_3+\text{Al}_2\text{O}_3)\times 100$, in mol.) are also often used (e.g., Gao et al., 2002; Handler et al., 2003; Wu et al., 2006; Armytage et al., 2014; Byerly and Lassiter, 2012). Most fertility proxy correlations can be interpreted by both partial melting and refertilization processes, but there are exceptions. Elthon (1992) showed that the linear relationship between Na_2O and MgO observed in abyssal peridotites was inconsistent with partial melting, but could be explained by refertilization. In addition, variations of major, minor and trace elements through the harzburgite-lherzolite contacts in the Lherz massif indicate that the lherzolites were formed through a refertilization process (Le Roux et al., 2007). The refertilization mechanism also provides a key to understanding the paradoxical association of light rare earth element (LREE) enrichment with depleted harzburgite often observed in mantle xenoliths and in tectonically-emplaced peridotites (e.g., Frey and Prinz, 1978; McDonough and Frey, 1989; Godard et al., 1995; Le Roux et al., 2007; Tilhac et al., 2021). Finally, radiogenic isotope signatures, such as those of Hf, Nd, Sr and

Os (e.g., Saal et al., 2001; Müntener et al., 2004; Le Roux et al., 2009, 2016; Lawley et al., 2020; Borghini et al., 2021; Reisberg, 2021), have often been attributed to the effects of refertilization, though this effect may be indirect, reflecting radiogenic ingrowth following ancient enrichment. For instance, the negative correlation of $^{87}\text{Sr}/^{86}\text{Sr}$ with Al_2O_3 and the positive correlation of $^{143}\text{Nd}/^{144}\text{Nd}$ with Al_2O_3 observed in Pyrenean peridotites (Downes et al., 1991; Bodinier & Godard, 2003) probably result from refertilization, with the most likely scenario being radiogenic decay following ancient enrichment in incompatible elements by a percolating melt with a depleted (MORB-like) isotopic composition (Le Roux et al., 2007). Similarly, frequently observed positive correlations between $^{187}\text{Os}/^{188}\text{Os}$ and Al_2O_3 in lithospheric peridotites may reflect radiogenic ingrowth after refertilization occurring soon after ancient melting events (Reisberg, 2021).

Formation of lherzolites by refertilization of depleted harzburgite during percolation of a silicate melt is frequently proposed to explain the composition of peridotite suites, notably in the Lherz massif (Pyrénées, France), type-locality of lherzolites (Le Roux et al., 2007), but also in numerous other worldwide occurrences including the Western Gneiss Region of Norway (Beyer, 2006), abyssal peridotites (Elthon, 1992; Seyler et al., 2007), or peridotite suites from the Kaapvaal craton (Simon et al., 2007) among other examples. Given the Os isotope evidence that large-scale refertilization can be temporally associated with the melting event that led to harzburgite depletion, refertilization is sometimes viewed as an integral part of the melting process, and has been described as “autometasomatism” (Rudnick and Walker, 2008). When melt circulation in the mantle is more channelized, cumulative pyroxenites may form (Bodinier et al., 2008; France et al., 2015; Tilhac et al., 2016; Borghini et al., 2020; Dai et al., 2021); such pyroxenites are among the most fertile mantle lithologies, and could thus be important components in any potential subsequent partial melting episode (e.g., Lambart et al., 2013; France et al., 2015).

An improved knowledge of refertilization of lithospheric peridotites is critical to understanding how the continental lithosphere developed its current composition. In this contribution, we investigate the influence of various parameters such as pressure, temperature, and redox conditions, as well as the chemical composition of the initial peridotite and percolating melt on the chemical and modal

composition of the resulting solid phase, using a thermodynamically based mixing model. Our model considers lithospheric processes related to the percolation of melts formed in the major melting regime, and does not explore the related processes with strongly silica-undersaturated liquid that form near the solidus under oxidized conditions (e.g., on the carbonated peridotite solidus). A similar approach (thermodynamic model of peridotite impregnation by a silicate melt) has been adopted by [Lambart et al. \(2012\)](#) and [Shaw et al. \(2018\)](#). [Lambart et al. \(2012\)](#) produced a simplified model of impregnation of a peridotite by a pyroxenite-derived melt at constant P and T, resulting in the generation of various peridotitic and pyroxenitic lithologies with systematic production of clinopyroxene. [Shaw et al. \(2018\)](#) were able to produce wehrlites by addition of orthopyroxene-undersaturated mafic alkaline magma to orthopyroxene bearing peridotite, followed by isobaric equilibration. While our approach is not entirely new, the goal of this paper is to determine the minimal number of parameters required to explain the SCLM compositional variability, as well as to confirm if the current understanding of the refertilization process is thermodynamically viable. The main goal of this paper is to determine whether a simple mixing model can reproduce both the bulk composition and the modal proportions of non-cratonic SCLM peridotites. Although simple (and therefore incomplete), our model is consistent with a global database of orogenic peridotites ([Bodinier and Godard, 2014](#)).

2. Approach

In this section, we reproduce the two end-member models: (1) mixing at constant P-T-fO₂ conditions during which a fixed mass of melt is progressively added to a refractory peridotite, and (2) partial melting of a fertile lherzolite.

2.1. pHMELTS and Adibat-1ph

In this study, we aim to test if the refertilization of a refractory peridotite by a silicate melt can explain the range of modal proportions observed in global non-cratonic lithospheric peridotites. We used the thermodynamic model pHMELTS ([Asimow et al., 2004](#)) and the adiabat-1ph front end ([Smith & Asimow, 2005](#)) to model the effects of magma impregnation in peridotites at constant pressure,

temperature and oxygen fugacity. The pHMELTS model calculates equilibrium assemblages in peridotitic systems by minimizing the Gibbs energy of the system from constraints on bulk composition, temperature, pressure or volume, enthalpy or entropy, and/or oxygen fugacity. The pHMELTS routine is part of the MELTS group of algorithms (Ghiorso & Sack, 1995). These algorithms are used to model mantle melting and magma crystallization, and also allow for melt-rock impregnation models. We use the pHMELTS software as it is suitable for pressures comprised between 1 and 3 GPa (Hirschmann et al., 1998), relevant for the non-cratonic SCLM.

The interface adiabat-1ph (Smith & Asimow, 2005) allows the automation of pHMELTS calculations. It is used to calculate equilibrium assemblages along a thermodynamic path. In particular, we used the ‘Adiabat assimilate’ option of the front-end to simulate the impregnation process as it allows us to add a fixed mass of melt after each calculation stage at constant P and T conditions. The output parameters (e.g., phase proportions and compositions) are calculated at each step along the thermodynamic path after equilibrium conditions are achieved.

The use of pHMELTS is subject to certain constraints due to the proven limits of the software:

- The subsolidus routines do not handle K₂O well if feldspar is not present (Asimow & Ghiorso, 1998). We therefore did not consider potassium.
- The incorporation of chromium is oversimplified. It does not enter into the modeled composition of pyroxenes and garnets (Asimow et al., 1995), which leads to an overestimation of the range of conditions for which spinel can crystallize (e.g., Lambart et al., 2009). In our calculations, we did include chromium due to the importance of spinel in the reaction but we considered the overestimation of spinel in the interpretation of the results.
- pHMELTS offers a choice between two thermodynamic models for garnet. The older model tends to overestimate the proportion of the grossular component (Berman & Koziol, 1991), while the new one tends to overestimate the stability range for garnet (e.g., Elkins et al., 2019). In our calculations, we used the older model of garnet but we performed calculations at a maximum pressure of 2 GPa to avoid the garnet stability field.

- The solidus temperatures of peridotites are overestimated (Ghiorso et al., 2002).

2.2. The mixing model

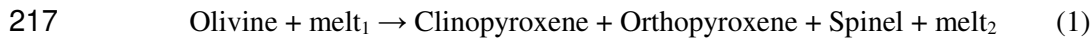
We consider a simple model in which a subsolidus homogenous mantle domain composed of depleted peridotite (harzburgite) is impregnated by a finite amount of melt at constant pressure and temperature. The impregnation process is simulated by adding up to 50 g of melt by increments of 0.01 g, to 100 g of depleted peridotite. Each incremental addition of melt is followed by chemical re-equilibration of the impregnated peridotite. [Lambart et al. \(2012\)](#) used a similar approach to investigate the fate of pyroxenite-derived melt during interaction with the surrounding peridotite, with larger increments (5g). We do not model melt percolation, but simply melt-peridotite interaction during melt addition; the implications of this limitation are discussed below. Our model also does not aim to reproduce the physical aspects of the refertilization process. The actual amount of melt required during the refertilization process is controlled by factors such as the degree of disequilibrium ([Oliviera et al., 2020](#)), the mobility of the melt ([Watson et al., 1990](#)), the pressure gradient ([Pec et al., 2015](#)), or the grain size of the protolith ([Turner et al., 2015](#)). It is beyond the scope of this paper to test the effects of such parameters. Here we focus on the major element and modal composition of the solid phases after interaction.

2.2.1. Selected input parameters

Pressure, temperature and oxygen fugacity: We selected a range of oxygen fugacity (fO_2) between FMQ-3 and FMQ +3 (with FMQ standing for the fayalite-magnetite-quartz oxygen buffer) to look at the effects of oxygen fugacity variations around the average value for the oceanic lithosphere ([Cottrell et al., 2021](#); [Foley, 2011](#)). Calculations were performed at 1.5 and 2 GPa, for temperatures (T) varying between 1150 and 1300°C, conditions corresponding to the subsolidus lithospheric mantle ([Hirschmann, 2000](#)). Under these conditions, silicate melts are expected to be strongly consumed during the reaction, for any realistic melt composition ([Lambart et al., 2012](#)). Details of the conditions for each test are given in **Table 1** (runs #1 to #12).

208 *Harzburgite compositions:* We selected three natural samples of depleted peridotites from the Lherz
209 massif (Roux et al. 2007) as starting compositions (Table 2). H1 corresponds to an average
210 harzburgite, H2 is slightly enriched in orthopyroxene, and H3 is orthopyroxene-rich.

211 *Melt compositions:* Several experimental studies have shown that a large part of the mineralogical and
212 compositional diversity in the mantle can be explained by melt-rock reactions (e.g., Kelemen et al.,
213 1990; Yaxley and Green, 1998; Morgan and Liang, 2003, 2005; Herzberg 2011; Lambart et al., 2012;
214 Mallik and Dasgupta, 2013; Soustelle et al., 2014; Mitchell & Grove, 2016). Le Roux et al. (2007)
215 suggested a refertilization process as a melt-rock reaction resulting in the dissolution of olivine and
216 crystallization of pyroxenes and spinel:



218 Not every melt, however, can trigger reaction (1) as the silica activity of the interacting melt must be
219 higher than the silica activity of the melt in equilibrium with the harzburgite protolith (Lambart et al.,
220 2012). If the silica activity is lower, clinopyroxene and olivine are produced at the expense of
221 orthopyroxene. For instance, Shaw et al. (2018) interpreted the formation of wehrlite as the result of
222 infiltration of orthopyroxene-undersaturated alkaline melt into the lithospheric mantle. The silica
223 activity calculated (Ghiorso et al., 1995) for the melt used in their model is low (e.g., $a_{\text{liq}}^{\text{SiO}_2} \sim 0.2$ at P
224 = 1.25 GPa and $T = 1350^\circ\text{C}$, and FMQ). In comparison, under similar conditions, the silica activity of
225 a melt in equilibrium with orthopyroxene and olivine is ~ 0.35 (Lambart et al., 2012).

226 In our calculations, we used three different basaltic melts (Table 3). The MOR melt is a basaltic
227 composition with a silica activity of 0.372, obtained in a partial melting experiment of a fertile
228 peridotite (Lambart et al., 2009) and corresponds to a spreading-ridge context. HS and HS2 are
229 picritic basalt compositions from Hawaii (Kilauea; Norman & Garcia, 1999) and Iceland (Reykjanes
230 Peninsula; Jakobsson, 1978), respectively. In our calculations, they represent primitive magmas from
231 hot spot contexts, with HS being more iron-rich than HS2. Unlike HS (which is olivine-rich), HS2
232 contains almost no phenocrysts and thus more closely represents a melt composition.

233 The silica activity of HS and HS2 melts are 0.485 and 0.551, respectively. Both of these melts have
234 higher silica activity than an experimental melt produced from partial melting of a fertile spinel
235 lherzolite at 2 GPa and 1375 °C, which has a value (i.e., 0.370; see KLB-1 run #21; [Hirose &](#)
236 [Kushiro, 1993](#)) very similar to that of the MOR melt.

237 For the P-T conditions chosen for the calculations, the liquid is completely, or very nearly (runs #3
238 and #5), consumed during the reaction. The strong consumption of silicate melt is partly due to the
239 overestimation of the solidus temperatures in pHMELTS ([Ghiorso et al., 2002](#)), regardless of the
240 composition (or silicate activity) of the melt and is also supported by experimental studies (e.g.,
241 [Yaxley and Green, 1998](#); [Lambart et al., 2012](#)). It results in an enrichment of the incompatible
242 element concentration in the produced solid. When the liquid is absent after equilibration, the system
243 can be viewed as a two-component mixture between the depleted peridotite and the added melt.

244 As the melt consumption is usually accompanied by the precipitation of clinopyroxene
245 (+orthopyroxene/olivine), it results in a local decrease in the permeability of the system. [Lambart et](#)
246 [al. \(2012\)](#) suggested that such permeability decrease might result in the affected lithology evolving as
247 a near-closed system, similar to what is modeled here. Nevertheless, a silicate melt in mineralogical
248 assemblages dominated by olivine can however become interconnected at a very low melt fraction
249 (e.g., [Waff & Faul, 1992](#); [Zhu et al., 2011](#); [Laumonier et al., 2017](#)), and a real closed system is
250 unlikely. The escape of a small melt fraction has however very little impact on the behavior of
251 elements with an affinity for the solid phase (i.e., the compatible elements), but can significantly
252 affect elements preferentially partitioning into the melt phase (i.e., incompatible elements). The latter
253 should thus be preferred if we are to characterize the open/closed character of the process. In order to
254 test the impact of the presence of a melt phase on the incompatible element concentrations of the
255 coexisting solid phase, we also performed a run with a liquid phase present (run #12, **Table 1**).
256 Calculations were performed at $T = 1400^{\circ}\text{C}$, an unlikely temperature for the continental lithosphere,
257 which forced the resulting system to have a melt phase. In this melt-present run, the incompatible
258 elements are partitioned into the melt phase during each step of the modeled process. While the closed
259 system approximation underscores the simplicity of our model and its limited applicability to

incompatible element concentrations, in many aspects our calculations may be representative of a process of simple impregnation of a refractory peridotite by a silicate melt in the continental mantle lithosphere.

2.3. The partial melting model

In order to compare with the impregnation model, we also performed 3 partial melting simulations (runs PM1, PM2 and PM3, **Table 1**). We used the Primitive Upper Mantle composition from [McDonough \(1995\)](#) as a starting composition (PUM in **Table 2**). Run PM1 was performed at constant pressure (2 GPa), with a temperature rising from 1200 to 1520°C. Run PM2 was performed at constant temperature (1230°C), with pressure decreasing from 2 to 0.6 GPa. Finally, run PM3 was performed at constant entropy, with pressure decreasing from 2 to 0.6 GPa, and starting temperature of 1396°C (PUM solidus temperature at 2 GPa), in order to model more geodynamically realistic conditions. As the melt remains in contact with the residue throughout the simulations, all three of these cases can be viewed as thermodynamically constrained batch melting models.

3. Results

We focus on the solid bulk composition and modal proportions of the solid phase and do not consider mineral phase compositions. In fact, inter-mineral partitioning of major element components such as Fe-Mg in the lithospheric mantle is strongly dependent on the equilibration temperature ([Brey and Köhler, 1990](#)). As thermal reequilibration is the rule in lithospheric domains, comparing the elemental compositions of the individual phases obtained from our thermodynamic model outputs with natural data would not produce meaningful results. Bulk residual assemblage compositions and modal proportions are less significantly affected by the temperature of reequilibration, and we present the corresponding results hereafter.

3.1. Reference simulation (run #1)

The main results of the mixing models are the evolutions of modal proportions (**Figs. 2, 3, Table 4, and Supplementary Fig. S1**), and of bulk solid assemblage compositions (**Fig. 4 and 5**). We will use

the outputs of run#1 as a reference for comparison with other tests. Results for this run show production of spinel (+2.5), orthopyroxene (+0.2), and clinopyroxene (+28.6), with the values indicating the absolute change in the modal proportion of each phase (normalized to 100). In contrast, the liquid is totally consumed and olivine proportion also diminishes (-31.3) (**Fig. 2**). This decrease in olivine proportion is not due solely to the precipitation of the other phases but also to olivine dissolution (Fig. 2b). Initial harzburgite is hence progressively modified to clinopyroxene-rich harzburgite, and eventually to a lherzolite assemblage (**Fig. 3**). As no liquid is present after equilibration, the bulk chemical composition of the solid assemblage (**Fig. 4**) evolves along mixing lines between the composition of the initial peridotite and the composition of the melt. Therefore, for run#1, after addition of 50% liquid, the bulk chemical composition shows an enrichment in Al_2O_3 (+5.4 wt.%), CaO (+3.8 wt.%), SiO_2 (+1.6 wt.%), and Na_2O (+1 wt.%), a decrease in MgO (-11.7 wt.%), and a slight decrease in FeO_t (-0.3 wt.%) (FeO_t : total iron content expressed as FeO).

3.2. Influence of the impregnation conditions

The effect of variations of P, T, and redox parameters on the model results are presented in **Fig. 3a**. Runs #1, #3 and #4 illustrate the effect of temperature on the reaction ($T = 1230, 1300$, and 1150°C , respectively), runs #1 and #5 are used to investigate the effect of a small variation of pressure ($P = 2$ and 1.5 GPa, respectively). Runs #1, #6a, #6b, #7a and #7b are used to track the effect of redox conditions on the reaction ($f\text{O}_2 = \text{FMQ}, \text{FMQ}+1, \text{FMQ}+3, \text{FMQ}-1$, and $\text{FMQ}-3$, respectively). In all of these cases, the same initial peridotite composition and the same melt composition were used (H1; MOR). The effect of pressure and temperature is insignificant for the ranges considered in this study (**Fig. 3a**). Additionally, for most of the $f\text{O}_2$ conditions tested here, the modal proportions of the impregnated peridotite strongly overlap with each other. Under highly oxidized conditions (i.e., run #6b: $\text{FMQ}+3$) however, 4.9 wt.% of orthopyroxene is produced at the expense of olivine (-35.3 wt.%). This is because Fe^{3+} is not easily incorporated in olivine and a higher $\text{Fe}^{3+}/\text{Fe}^{2+}$ ratio will favor the dissolution of olivine and precipitation of pyroxene.

3.3. Influence of the composition

The influence of the melt composition on the refertilization process was tested in runs #1, #2 and #11 (MOR, HS, and HS2, respectively). The influence of the initial peridotite composition was tested in runs #1, #8 and #9 (H1, H2, and H3, respectively). Run #10 also investigates a variation of both starting material composition (H3) and melt composition (HS). These six runs are displayed in **Figs. 3b, 3c and 4**. Because the melt is consumed during the reaction, bulk compositions follow mixing lines between the composition of the initial peridotite and the composition of the melt (**Fig. 4**). In the major element diagrams (**Fig. 4**), this results in solid assemblages with greater sodium and calcium enrichments for models performed with MOR addition, and slightly greater iron enrichment for models performed with HS addition, relative to that performed with HS2 addition, directly reflecting the differences in melt compositions (**Table 3**). In the Streckeisen projections (**Fig 3b**), the addition of the HS2 melt (run #11) results in a strong orthopyroxene enrichment and the final lithology (after 50% melt addition) is an orthopyroxene-rich olivine websterite (35% olivine, 52% orthopyroxene, 9% clinopyroxene). On the contrary, the reaction with the MOR melt (run #1) results in both clinopyroxene and orthopyroxene enrichments, but the final lithology is in the field of lherzolite (49% olivine, 20% orthopyroxene, 29% clinopyroxene). The addition of HS melt (run #2) results in a near-vertical trend in the Streckeisen diagram with a final lithology in the field of lherzolite with a similar proportion of olivine but a higher orthopyroxene/clinopyroxene ratio (49% olivine, 30% orthopyroxene, 20% clinopyroxene). Finally, the main effect of varying the initial harzburgite composition is to change the initial location of the mixing trend, that is the orthopyroxene/olivine ratio in the Streckeisen projection (**Fig. 3c**). Runs #1 and #8 evolve from the domain of harzburgites to lherzolites, and run #9 to websterites.

3.4. Other runs

3.4.1 Partial melting runs

Partial melting simulations PM1, PM2 and PM3 are presented in **Fig. 3d** and **Fig. 5**. The end of run PM1 corresponds to an amount of liquid produced of 30 wt.% (**Table 4, Supplementary Fig. S1n**), while the ends of PM2 and PM3 correspond to 7 wt.% and 5 wt.% of liquid produced, respectively

337 (Supplementary Figs. S1o and S1p). The low amount of melt produced in PM2 and PM3 is due to
338 the overestimation of the solidus temperature of the peridotite in pHMELTS (Ghiorso et al., 2002). In
339 the partial melting run at constant pressure (PM1), as the temperature rises above the PUM (Primitive
340 Upper Mantle; McDonough, 1995) solidus temperature at 2 GPa (1296°C), clinopyroxene is strongly
341 consumed (-22 modal %) corresponding to a change in lithology from lherzolite to harzburgite (Fig.
342 3d). The chemical composition of the residual solid shows a final enrichment in MgO (+6 wt.%), and
343 SiO₂ (+0.8 wt.%), associated with a decrease in Al₂O₃ (-2.5 wt.%), CaO (-2.5 wt.%), FeO_t (-1.4
344 wt.%), and Na₂O (-0.3 wt.%), with values representing absolute changes in the proportions of these
345 species in the solid phase. In the plot of Na₂O vs. Al₂O₃ a curved trend is observed, which starts out
346 steeply at Al₂O₃ contents > 4 wt.%, and Na₂O contents > 0.1 wt.% and flattens out with continued
347 melting (Fig. 5).

348 The partial melting run under conditions of isentropic decompression (PM3) also starts at 1296°C.
349 pHMELTS adapts the temperature during the simulation in order to maintain constant entropy (down
350 to 1214°C). By the end of the run, olivine has been produced (+2.4%) at the expense of clinopyroxene
351 (-8.6 %) (Fig. S1p). However, in detail some complexity is observed as pressure decreases. At first
352 the formation of orthopyroxene (+1.6 %) is slightly favored over that of olivine (+1.1%), but starting
353 at around 0.8 GPa, the orthopyroxene/olivine ratio shows a progressive decrease, as olivine
354 production is favored in comparison to orthopyroxene (Fig. 3d), consistent with the increasing
355 stability of olivine with decreasing pressure (Stolper, 1980). The chemical composition of the residual
356 solid shows an enrichment in MgO (+2 wt.%) and FeO_t (+0.2 wt.%), and a decrease in Al₂O₃ (-1
357 wt.%), SiO₂ (-0.6 wt.%), CaO (-0.3 wt.%), and Na₂O (-0.3 wt.%) (Fig. 5).

358 The partial melting run by decompression at constant T (PM2) shows similar evolution to that at
359 constant entropy (PM3). Olivine is produced (+3%) at the expense of clinopyroxene (-5.5%) and
360 orthopyroxene (-4.3%) (Fig. 3d and Supplementary Fig. S1o). The residual solid is enriched in MgO
361 (+2.36 wt.%) and FeO_t (+0.25 wt.%), and depleted in Al₂O₃ (-1.2 wt.%), SiO₂ (-0.7 wt.%), CaO (-0.4
362 wt.%), and Na₂O (-0.28 wt.%) (Fig. 5). In runs PM2 and PM3, the relatively limited change in bulk

composition, which does not attain the harzburgite field, is likely due to the overestimation of the solidus temperature in pHMELTS noted above.

3.4.2. Liquid-present run

In most respects, the liquid-present run#12 (**Figs. 3d and 5**) shows a similar trend to the runs performed at lower temperature. A notable exception is Na content, which is less enriched in the refertilized assemblage than in the melt-free models (+0.4 wt.% for run #12, compared to +1 wt.% for the reference run). This is because Na is strongly partitioned into the liquid phase. The final percentage of melt in the assemblage is 7.5 wt.%. Minor amounts of liquid are also present in runs #3 (1300°C) and #5 (1.5GPa) and these also show a slightly lower Na enrichment in the solid assemblage than in the melt-free runs. Nevertheless, the final melt fractions being 0.9 wt.% and 1.6 wt.% (respectively) in these runs, the variation of the Na content compared to the reference simulation is not significant (+0.8 wt.% and +0.7 wt.% for runs #3 and #5 respectively, compared to +1 wt.% for the reference run). For the other chemical elements, these two runs show similar trends to those of the reference run.

4. Discussion

Refertilization of the SCLM is a complex phenomenon that likely involves numerous agents and mechanisms. Nevertheless, our model confirms that the reaction: Olivine + melt₁ → Clinopyroxene + Orthopyroxene + Spinel + melt₂ suggested based on petrological grounds (e.g., [Le Roux et al., 2007](#)) is thermodynamically possible, and thus supports its key participation in the refertilization process. The composition of the infiltrating melt has a first-order control on the range of chemical and mineralogical compositions observed in the SCLM.

4.1. Natural data

Most ophiolitic and abyssal peridotites are represented by harzburgitic lithologies (e.g., [Bodinier and Godard, 2014](#)). On the contrary, peridotites from the sub-continental lithosphere, particularly orogenic peridotites and ultramafic xenoliths from non-cratonic terrains, encompass many lherzolic

lithologies (**Fig. 3**). There is substantial scatter in natural peridotite chemical compositions (**Fig. 4 and 5**). However, most natural compositions define a broad trend, with increasing SiO_2 , CaO , Al_2O_3 and Na_2O contents, coupled with decreasing MgO content and relatively constant FeO content. Some of the scatter in modal and chemical composition in lithospheric peridotites could be due to inherited heterogeneity from the convecting mantle, related to crustal recycling, convection and melting, and melt-solid interactions beneath the ridges and at hot spots (e.g., [Sobolev et al., 2005](#)), or various degrees of partial melting under various conditions (e.g., melting at different pressures; [Olivera et al., 2020](#); [Tomlinson & Kamber, 2021](#)). Also temperature reequilibration could trigger noticeable modal variations in some specific samples (e.g., two-pyroxene exsolutions, pyroxene exsolution from garnet, spinel exsolution from clinopyroxene; [Kornprobst et al., 1990](#); [France et al., 2015](#)), which could also trigger scatter in the database, and that would eventually hamper direct comparison with our model outputs for those specific samples. However, the presence of a trend in major element compositions (**Figs. 4 and 5**) strongly suggests a genetic link between refractory (i.e., harzburgite) and fertile (i.e., lherzolite) lithologies. The goal of the following exercise is not to reproduce the full spectrum of natural compositions but to test whether our thermodynamic mixing model is consistent with this potential genetic link, and discuss which parameters in our model are the most likely to explain the spectrum of compositions observed in natural peridotites.

In **Figures 3, 4 and 5**, we compare the results of our thermodynamic mixing models with the global database for tectonically emplaced peridotites, including orogenic, ophiolitic and abyssal peridotites ([Bodinier and Godard, 2014](#)). Our results show that most of the wide range of modal proportions in lherzolite can be reproduced by our model of impregnation of harzburgitic lithologies by silicate melts. In addition, it is clear from **Fig. 3** that further impregnation would make the impregnated peridotite enter the domain of websterites, rocks composed essentially of orthopyroxene and clinopyroxene, and less than 40% olivine. This suggests that very extensive refertilization could be at the origin of some websterite and pyroxenites, and that harzburgites, lherzolites and pyroxenites may form a continuum rather than distinct groups. Such a continuum is commonly reported in mantle series and mainly explained by melt-rock reactions (e.g., from clinopyroxenite to orthopyroxenite in

Kornprobst, 1969; from dunite to lherzolite in Morgan and Liang, 2005; from dunite to websterite in Denis et al., 2018, or from harzburgite to websterite in Lambart et al., 2022). The simple impregnation model presented here however, is unlikely to explain the scatter in the most refractory lithologies (i.e., olivine-rich harzburgite and dunite). Indeed, scatter in natural peridotite compositions (Figs. 4 and 5) exceeds the range of variation in our impregnation model with some rare peridotites showing very high $\text{CaO}/\text{Al}_2\text{O}_3$ ratio or high FeO (>10 wt.%) concentrations. However, most of the natural compositions and the impregnation model results follow similar chemical trends. The effects of each input parameter of the model are discussed below.

4.2. Influence of varying parameters on the refertilization products

The impregnation models presented here highlight that variations of temperature and redox conditions, as well as small pressure variations have almost no impact on the evolution of the system in terms of modal composition (Fig. 3a). Hereafter we first discuss the two main parameters that influence the evolution of the system in our calculations: the composition of the percolating melt, and to a lesser extent the composition of the percolated harzburgite.

4.2.1. Percolated harzburgite composition

Although significant scatter is present in the natural data when compared to our models, our results show that a refertilization process has the potential to reproduce the harzburgite - lherzolite suites. The scatter in the orthopyroxene/olivine ratio in natural lherzolite series could be explained by a variation of the orthopyroxene/olivine ratio in the initial harzburgite (Fig. 3c). This scenario would require a large preexisting compositional variability of the refractory mantle, *before* impregnation. Harzburgite H3, for instance, is an orthopyroxene-rich harzburgite with a very low calcium content compared to aluminum that can be viewed as an extreme orthopyroxene-rich end-member.

Several processes could explain the origin of such compositional variability (variations of the orthopyroxene/olivine ratio). For instance, in the decompression runs (PM2 and PM3), the stabilities of olivine and orthopyroxene during the melting reaction change with pressure. The coexistence of

various residual harzburgites formed by partial melting at different pressures could result in different orthopyroxene/olivine ratios. The preexisting heterogeneity could also be due to the delamination of the cratonic lithospheric mantle into the convecting mantle, be a natural consequence of oceanic crust subduction into the convecting mantle, or result from the interaction of peridotite with an eclogite or pyroxenite-derived melt (e.g., Yaxley and Green, 1998; Tomlinson & Kamber, 2021).

4.2.2. Percolating melt composition

For the following discussion, we used H1, a typical harzburgite (Table 2) as the starting composition to examine the effect of melt composition on the output of the impregnation modeling (Figs. 3b and 4). Because all three percolating melts have high silica activities (Table 3), in all cases the proportion of pyroxenes increases during melt impregnation. However, the clinopyroxene/orthopyroxene ratio is strongly affected by the Ca content of the melt with more clinopyroxene produced for Ca-rich melts (Table 3, Fig. 3b). In addition to being Ca-poor, HS2 is also more Si-rich than the two other basalt compositions, resulting in more efficient crystallization of pyroxene, particularly orthopyroxene, at the expense of olivine (Fig. 3b and Supplementary Fig. S11). This results in a final mineralogical assemblage for run #11 in the field of orthopyroxene-rich olivine websterite.

Except for the liquid-present run (run #12), the melt phase is entirely, or almost entirely (runs #3 and #5; Supplementary Fig. S1b and S1d), consumed during the impregnation process (Table 4). This implies that the bulk composition of the percolated peridotite evolves along a mixing trend between the starting harzburgite and the melt composition (Fig. 4). We note that melt HS2 is too Ca-poor to reproduce the trend of natural compositions. Additionally, part of the vertical scatter for all oxides in Fig. 4 cannot be explained by our impregnation model (especially for ophiolitic and abyssal peridotites; e.g., variation of SiO_2 content for a given Al_2O_3 content). Finally, for the three melt compositions tested here, the modeled Na_2O vs. Al_2O_3 enrichment trend is much steeper than the correlation observed in the natural dataset (Fig. 4). As described in sections 2.2.1 and 3.4.2, this is due to the full consumption of liquid during the reaction, which likely differs from olivine-dominated systems in which a small fraction of liquid is expected to leave the system during melt percolation

(see reaction (1)). Without this liquid phase, elements that partition preferentially into the melt phase such as Na remain in the solid phases (**Fig. 4**). On the contrary, in the presence of a liquid phase (run #12), Na preferentially partitions into the melt resulting in a much lower increase of the Na₂O content in the solid phase during the impregnation process (**Fig. 5**), similar to the trend observed in natural data. In the liquid-present run, the final melt fraction in the system at equilibrium is about 7.5 wt.%. In natural systems, which may be seen as chromatographic percolation columns (e.g., [Navon and Stolper, 1987](#)), significantly lower instantaneous melt fractions can explain the low contents of Na in the solid phase. Chemical disequilibrium during melt transport also favors stronger partitioning of Na into the melt phase ([Oliveira et al., 2020](#)). In any case our results support the supposition that refertilization is an open system process.

4.3. Comparison with partial melting

Partial melting processes can also produce refractory lithologies (**Fig. 3d** and **Fig. 5**). However, our partial melting models do not fully reproduce the spectrum of compositions observed in non-cratonic continental peridotites (**Fig. 3d** and **Fig. 5**). In addition, our mixing model tended to reproduce the rough linear trend represented by the spectrum of natural continental lithospheric data more faithfully than our simplified partial melting model (straight line vs. curved lines for runs PM2 and PM3 in **Fig. 3d**). Previous authors (e.g. [Niu, 1997](#)) have also pointed out that mixing more successfully reproduces linear trends (FeO vs. MgO and SiO₂ vs MgO) in peridotites than partial melting alone. We note however, that more complex dynamic melting models, such as that of [Oliveira et al. \(2020\)](#) which takes into consideration disequilibrium behavior, heterogeneous source compositions and melt transport rates, can produce a wider variety of compositions than the partial melting runs performed in this study (**Fig. 3d**).

As highlighted in **Fig.1**, partial melting and refertilization likely both contribute to producing lithospheric heterogeneities. Furthermore, refertilization and partial melting sometimes may be genetically linked, as the near absence of lherzolites with unradiogenic osmium isotope compositions in the non-cratonic lithosphere argues that refertilization usually occurs soon after harzburgite

formation (Rudnick & Walker, 2008; Reisberg, 2021). This implies that the original partial melting episodes may potentially be causally linked to subsequent refertilization, which could result from percolation of the remaining melts through the cooling lithosphere. We stress that refertilization as used here refers to the process of transformation of harzburgite by interaction with silicate melt in the non-cratonic mantle lithosphere. This can produce clinopyroxene-enriched harzburgite, lherzolite, or other types of peridotite depending on the percolating melt composition. Other refertilization processes, often referred to broadly as metasomatic (e.g., circulation of various silicate melts, or of hydrous, carbonatitic, or kimberlite fluids/melts) also very frequently affect both the cratonic (e.g., Song and Frey, 1989; Griffin et al., 1999; Jollands et al., 2018) and the non-cratonic lithosphere (e.g., Menzies and Dupuy, 1991; Baker et al., 1998; Raffone et al., 2009; Gu et al., 2018; Azevedo-Vannson et al., 2021). Such processes can lead to enrichment of major or incompatible element abundances, water contents, modification of isotope compositions and/or localized phase precipitation, and can occur at various times throughout the history of a lithospheric domain.

4.4. Other parameters.

One of the goals of our study was to determine the first-order parameters controlling the compositional and modal variability of the SCLM. Unsurprisingly, the melt and the protolith compositions have the strongest effect on the evolution of the system. However, because of the simplicity of our model, the effects of other parameters (e.g., fO_2 , presence of volatiles, chemical disequilibrium), may be underestimated. Here we briefly review the potential effects of additional parameters.

Our results show that highly oxidized melts result in slightly higher olivine dissolution and slightly higher pyroxene (mostly orthopyroxene) precipitation compared to the reference run (see run #6b: Fig. 3a). Such high degrees of oxidation have been encountered in some oceanic island xenoliths (Cottrell et al., 2021) and might reflect the interaction of the xenolith with a hydrous melt (e.g., Bryant et al., 2007). However, for most conditions relevant to the lithospheric mantle, and in the major melting regime considered in this study, the effect of fO_2 seems to be insignificant. These

results are consistent with [Shaw et al. \(2018\)](#). In their calculations, an increase in the fO_2 from FQM-2 to FQM+2 resulted in a small decrease of the olivine/orthopyroxene ratio in the initial lithology but the effect of variable fO_2 on the output of the reaction was negligible.

The addition of volatiles (H_2O or CO_2) is expected to significantly decrease the solidus temperature of the system (e.g., [Asimow and Langmuir, 2003](#); [Dasgupta and Hirschmann, 2006](#)). Hence, based on temperature considerations only, we could expect that a refertilizing hydrous or carbonated melt would result in lower consumption of melt during the reaction. However, this is not supported by experiments. [Mallik and Dasgupta \(2013\)](#) performed reaction experiments between a lherzolite and a CO_2 -bearing basaltic andesite melt. In comparison to similar CO_2 -free experiments, the addition of CO_2 to the reacting melt has little to no effect on the proportion of residual melt after the reaction. This likely is because the addition of volatiles in the melt increases the reactivity and disequilibrium degree of the melt, resulting in a highly dynamic dissolution-precipitation process (e.g., [Keller and Katz, 2016](#); [Lambart et al., 2022](#); [Mallmann et al., 2009](#); [Shaw et al., 2018](#)). Additionally, in comparison to CO_2 -free experiments, [Mallik and Dasgupta \(2013\)](#) observed an increase in orthopyroxene (and garnet) in the residual solid after reaction at the expense of olivine and clinopyroxene. Similarly, [Wang et al. \(2016\)](#) demonstrated that the reaction of a hydrous melt with a lherzolite can produce orthopyroxenite. Hence, although orthopyroxene stability also strongly depends on the silica activity of the melt, the addition of volatiles may result in shifting the compositional effect of the melt towards orthopyroxene-rich lithologies (**Fig. 3**). However, the effect of volatiles is likely limited in comparison to that of the major-element composition of the melt. In fact, in the [Mallik and Dasgupta \(2013\)](#) study, similar experiments performed with an alkali basalt melt, but with a CO_2 content more than four times higher than that of the basaltic andesite melt result in much lower consumption of olivine for a similar consumption of melt.

[Oliveira et al. \(2020\)](#) demonstrated that the degree of chemical disequilibrium during partial melting can significantly modify the compositional trends of major elements observed in basalt when compared with equilibrium calculations. As these authors noted, disequilibrium polybaric melting increases the fractionation of Na into the melt phase. In their calculations however, both equilibrium

and disequilibrium models produced similar modal evolution of the residual mantle (**Fig. 3d**). The effect of variable potential temperature of the mantle can result in slightly larger variability, but mostly because it results in changing the initial mineralogical composition of the lherzolite between the spinel and the garnet stability field.

5. Conclusions

In order to test the hypothesis of lherzolite formation by refertilization of the non-cratonic continental mantle lithosphere, we employed a simple thermodynamic mixing model of harzburgite with a silicate melt of tholeiitic to picritic composition. We independently investigated the influence of various thermodynamic parameters (pressure, temperature, redox conditions, and the chemical composition of initial peridotite and percolating melt) on the chemical and modal compositions of the resulting lithology. Despite their simplicity, our calculations show that a large part of the compositional variability observed in orogenic peridotites can be explained by the impregnation of a refractory harzburgitic lithospheric mantle with silicate melt of various compositions. We also show that temperature, oxygen fugacity, and small variations of pressure have almost no impact on the evolution of the modal composition of the system; melt composition and initial harzburgite composition are the most influential thermodynamic parameters. The latter directly control the refertilization reaction and so, the phase proportions. To reproduce the natural compositional variability of continental peridotites, initial compositional heterogeneity of the harzburgitic protoliths is needed, as well as impregnation with various silicate melts. The three liquid compositions used here represent a range of mantle melts that could serve as potential refertilizing agents. Our run #2 with an initial average harzburgitic composition (H1) and a picritic basaltic melt (HS) best reproduced the broad trend of the natural data, but other protolith-melt combinations could also explain some of the natural variability. For instance, the composition of a liquid depends on its geodynamic context, which controls the pressure and temperature of melting, as well as the composition of the source. Finally, we highlighted that the main limitation of our model is that the refertilization process is treated as simple melt impregnation rather than melt percolation. The elements that partition preferentially into the melt phase (represented here by Na) are removed from the rock during melt percolation in the natural

system. Our thermodynamic mixing model cannot reproduce this strong fractionation of incompatible elements in the liquid phase during reactive infiltration as in our model, the melt phase is completely consumed in the reaction. This leads to an enrichment of incompatible elements in the resulting lithology in the model, and underscores the open system character of the natural refertilization process. Despite this drawback, our calculations provide thermodynamic support for models suggesting that much of the variability in the major element and modal compositions of the natural data can be reproduced by the impregnation of a harzburgite with silicate melts of various compositions.

Acknowledgments

We thank the reviewers, Cliff Shaw and Romain Tilhac, for their constructive comments, as well as Sonja Aulbach for her editorial handling, which greatly improved the quality of this manuscript. LF thanks Pierre Bouilhol, Jean-Louis Bodinier, and Valentin Casola for constructive discussions related to mantle refertilization. This work was supported by the French National Research Agency through the project GECO-REE (ANR-16-CE01-0003-01; P.I., LF). SL acknowledges funding support from NSF grant EAR-1946346. This is CRPG contribution number xxxx, and GECO-REE contribution number yy.

References

- Allègre, C. J., & Turcotte, D. L. (1986). Implications of a two-component marble-cake mantle. *Nature*, 323(6084), 123-127. <https://doi.org/10.1038/323123a0>
- Armytage, R. M. G., Brandon, A. D., Peslier, A. H., & Lapen, T. J. (2014). Osmium isotope evidence for Early to Middle Proterozoic mantle lithosphere stabilization and concomitant production of juvenile crust in Dish Hill, CA peridotite xenoliths. *Geochimica et Cosmochimica Acta*, 137, 113-133. <https://doi.org/10.1016/j.gca.2014.04.017>
- Asimow, P. D., Dixon, J. E., & Langmuir, C. H. (2004). A hydrous melting and fractionation model for mid-ocean ridge basalts: Application to the Mid-Atlantic Ridge near the Azores: HYDROUS MELTING AND FRACTIONATION. *Geochemistry, Geophysics, Geosystems*, 5(1), n/a-n/a. <https://doi.org/10.1029/2003GC000568>

597 Asimow, P. D., & Ghiorso, M. S. (1998). Algorithmic modifications extending MELTS to calculate subsolidus phase
 598 relations. *American Mineralogist*, 83(9-10), 1127-1132. <https://doi.org/10.2138/am-1998-9-1022>

599 Asimow, P. D., & Langmuir, A. C. (2003). The importance of water to oceanic mantle melting regimes. *Nature*, 421(6925),
 600 815-820.

601 Asimow, P. D., Hirschmann, M. M., Ghiorso, M. S., O'Hara, M. J., & Stolper, E. M. (1995). The effect of pressure-induced
 602 solid-solid phase transitions on decompression melting of the mantle. *Geochimica et Cosmochimica Acta*, 59(21),
 603 4489-4506. [https://doi.org/10.1016/0016-7037\(95\)00252-U](https://doi.org/10.1016/0016-7037(95)00252-U)

604 Azevedo-Vannson, S., France, L., Ingrin, J., Chazot, G. (2021) Mantle metasomatic influence on water contents in
 605 continental lithosphere: New constraints from garnet pyroxenite xenoliths (France & Cameroon volcanic provinces).
 606 *Chemical Geology*, 575, 1202257.

607 Baker, J., Chazot, G., Menzies, M., & Thirlwall, M. (1998). Metasomatism of the shallow mantle beneath Yemen by the
 608 Afar plume—Implications for mantle plumes, flood volcanism, and intraplate volcanism. *Geology*, 26(5), 431.
 609 [https://doi.org/10.1130/0091-7613\(1998\)026<0431:MOTSMB>2.3.CO;2](https://doi.org/10.1130/0091-7613(1998)026<0431:MOTSMB>2.3.CO;2)

610 Berman, R. G., & Koziol, A. M. (1991). Ternary excess properties of grossular-pyropes-almandine garnet and their influence
 611 in geothermobarometry. *American Mineralogist*, 76(7-8), 1223-1231.

612 Beyer, E. E. (2006). Transformation of Archaean Lithospheric Mantle by Refertilization: Evidence from Exposed
 613 Peridotites in the Western Gneiss Region, Norway. *Journal of Petrology*, 47(8), 1611-1636.
 614 <https://doi.org/10.1093/petrology/egl022>

615 Bodinier, J.-L., Garrido, C. J., Chanéfo, I., Bruguier, O., & Gervilla, F. (2008). Origin of Pyroxenite-Peridotite Veined
 616 Mantle by Refertilization Reactions: Evidence from the Ronda Peridotite (Southern Spain). *Journal of Petrology*, 49(5),
 617 999-1025. <https://doi.org/10.1093/petrology/egn014>

618 Bodinier, J.-L., & Godard, M. (2003). Orogenic, Ophiolitic, and Abyssal Peridotites. In *Treatise on Geochemistry* (p. 1-73).
 619 Elsevier. <https://doi.org/10.1016/B0-08-043751-6/02004-1>

620 Bodinier, J.-L., & Godard, M. (2014). Orogenic, Ophiolitic, and Abyssal Peridotites. In *Treatise on Geochemistry* (p.
 621 103-167). Elsevier. <https://doi.org/10.1016/B978-0-08-095975-7.00204-7>

622 Borghini, G., Rampone, E., Class, C., Goldstein, S., Cai, Y., Cipriani, A., Hofmann, A. W., & Bolge, L. (2021). Enriched Hf
 623 Nd isotopic signature of veined pyroxenite-infiltrated peridotite as a possible source for E-MORB. *Chemical Geology*, 586,
 624 120591. <https://doi.org/10.1016/j.chemgeo.2021.120591>

625 Borghini, G., Rampone, E., Zanetti, A., Class, C., Fumagalli, P., & Godard, M. (2020). Ligurian pyroxenite-peridotite
626 sequences (Italy) and the role of melt-rock reaction in creating enriched-MORB mantle sources. *Chemical Geology*, 532,
627 119252. <https://doi.org/10.1016/j.chemgeo.2019.07.027>

628 Brey, G. P., & K Hler, T. (1990). Geothermobarometry in Four-phase Lherzolites II. New Thermobarometers, and Practical
629 Assessment of Existing Thermobarometers. *Journal of Petrology*, 31(6), 1353-1378.
630 <https://doi.org/10.1093/petrology/31.6.1353>

631 Byerly, B. L., & Lassiter, J. C. (2012). Evidence from mantle xenoliths for lithosphere removal beneath the central Rio
632 Grande Rift. *Earth and Planetary Science Letters*, 355-356, 82-93. <https://doi.org/10.1016/j.epsl.2012.08.034>

633 Bryant, J. A., Yogodzinski, G. M., & Churikova, T. G. (2007). Melt-mantle interactions beneath the Kamchatka arc:
634 Evidence from ultramafic xenoliths from Shiveluch volcano. *Geochemistry, Geophysics, Geosystems*, 8(4).

635 Chazot, G., Menzies, M., & Harte, B. (1996). Silicate glasses in spinel lherzolites from Yemen : Origin and chemical
636 composition. *Chemical Geology*, 134(1-3), 159-179. [https://doi.org/10.1016/S0009-2541\(96\)00086-1](https://doi.org/10.1016/S0009-2541(96)00086-1)

637 Cottrell, E., Birner, S. K., Brounce, M., Davis, F. A., Waters, L. E., & Kelley, K. A. (2021). Oxygen Fugacity Across
638 Tectonic Settings. In R. Moretti & D. R. Neuville (Éds.), *Geophysical Monograph Series* (1^{re} éd., p. 33-61). Wiley.
639 <https://doi.org/10.1002/9781119473206.ch3>

640 Dai, H.-K., Zheng, J.-P., Griffin, W. L., O'Reilly, S. Y., Xiong, Q., Ping, X.-Q., Chen, F.-K., & Lu, J.-G. (2021). Pyroxenite
641 Xenoliths Record Complex Melt Impregnation in the Deep Lithosphere of the Northwestern North China Craton. *Journal of*
642 *Petrology*, 62(2), egaa079. <https://doi.org/10.1093/petrology/egaa079>

643 Dasgupta, R., & Hirschmann, M. M. (2006). Melting in the Earth's deep upper mantle caused by carbon dioxide. *Nature*,
644 440(7084), 659-662.

645 Denis, C. M. M., Demouchy, S., & Alard, O. (2018). Heterogeneous hydrogen distribution in orthopyroxene from veined
646 mantle peridotite (San Carlos, Arizona): Impact of melt-rock interactions. *Lithos*, 302-303, 298-311.
647 <https://doi.org/10.1016/j.lithos.2018.01.007>

648 Dick, H. J. B., Fisher, R. L., & Bryan, W. B. (1984). Mineralogic variability of the uppermost mantle along mid-ocean
649 ridges. *Earth and Planetary Science Letters*, 69(1), 88-106. [https://doi.org/10.1016/0012-821X\(84\)90076-1](https://doi.org/10.1016/0012-821X(84)90076-1)

650 Downes, H., Bodinier, J.-L., Thirlwall, M. F., Lorand, J.-P., & Fabries, J. (1991). REE and Sr-Nd Isotopic Geochemistry of
651 Eastern Pyrenean Peridotite Massifs : Sub-Continental Lithospheric Mantle Modified by Continental Magmatism. *Journal of*
652 *Petrology*, Special_Volume(2), 97-115. https://doi.org/10.1093/petrology/Special_Volume.2.97

653 Elkins, L. J., Bourdon, B., & Lambart, S. (2019). Testing pyroxenite versus peridotite sources for marine basalts using U-
654 series isotopes. *Lithos*, 332-333, 226-244. <https://doi.org/10.1016/j.lithos.2019.02.011>

655 Elthon, D. (1992). Chemical trends in abyssal peridotites: Refertilization of depleted suboceanic mantle. *Journal of*
656 *Geophysical Research*, 97(B6), 9015. <https://doi.org/10.1029/92JB00723>

657 Foley, S. F. (2011). A Reappraisal of Redox Melting in the Earth's Mantle as a Function of Tectonic Setting and Time.
658 *Journal of Petrology*, 52(7-8), 1363-1391. <https://doi.org/10.1093/petrology/egq061>

659 France, L., Chazot, G., Kornprobst, J., Dallai, L., Vannucci, R., Grégoire, M., Bertrand, H., & Boivin, P. (2015). Mantle
660 refertilization and magmatism in old orogenic regions: The role of late-orogenic pyroxenites. *Lithos*, 232, 49-75.
661 <https://doi.org/10.1016/j.lithos.2015.05.017>

662 Frey, F. A., John Suen, C., & Stockman, H. W. (1985). The Ronda high temperature peridotite: Geochemistry and
663 petrogenesis. *Geochimica et Cosmochimica Acta*, 49(11), 2469-2491. [https://doi.org/10.1016/0016-7037\(85\)90247-9](https://doi.org/10.1016/0016-7037(85)90247-9)

664 Frey, F. A., & Prinz, M. (1978). Ultramafic inclusions from San Carlos, Arizona: Petrologic and geochemical data bearing
665 on their petrogenesis. *Earth and Planetary Science Letters*, 38(1), 129-176. [https://doi.org/10.1016/0012-821X\(78\)90130-9](https://doi.org/10.1016/0012-821X(78)90130-9)

666 Gao, S., Rudnick, R. L., Carlson, R. W., McDonough, W. F., & Liu, Y.-S. (2002). Re-Os evidence for replacement of
667 ancient mantle lithosphere beneath the North China craton. *Earth and Planetary Science Letters*, 198(3-4), 307-322.
668 [https://doi.org/10.1016/S0012-821X\(02\)00489-2](https://doi.org/10.1016/S0012-821X(02)00489-2)

669 Garrido, C. J., & Bodinier, J.-L. (1999). Diversity of Mafic Rocks in the Ronda Peridotite: Evidence for Pervasive Melt-
670 Rock Reaction during Heating of Subcontinental Lithosphere by Upwelling Asthenosphere. *Journal of Petrology*, 40(5),
671 729-754. <https://doi.org/10.1093/petroj/40.5.729>

672 Ghiorso, M. S., & Sack, R. O. (1995). Chemical mass transfer in magmatic processes IV. A revised and internally consistent
673 thermodynamic model for the interpolation and extrapolation of liquid-solid equilibria in magmatic systems at elevated
674 temperatures and pressures. *Contributions to Mineralogy and Petrology*, 119(2-3), 197-212.
675 <https://doi.org/10.1007/BF00307281>

676 Ghiorso, M. S., Hirschmann, M. M., Reiners, P. W., & Kress, V. C. (2002). The pMELTS: A revision of MELTS for
677 improved calculation of phase relations and major element partitioning related to partial melting of the mantle to 3 GPa:
678 pMELTS, A REVISION OF MELTS. *Geochemistry, Geophysics, Geosystems*, 3(5), 1-35.
679 <https://doi.org/10.1029/2001GC000217>

Godard, M., Bodinier, J.-L., & Vasseur, G. (1995). Effects of mineralogical reactions on trace element redistributions in mantle rocks during percolation processes : A chromatographic approach. *Earth and Planetary Science Letters*, 133(3-4), 449-461. [https://doi.org/10.1016/0012-821X\(95\)00104-K](https://doi.org/10.1016/0012-821X(95)00104-K)

Godard, M., Joussetin, D., & Bodinier, J.-L. (2000). Relationships between geochemistry and structure beneath a palaeo-spreading centre : A study of the mantle section in the Oman ophiolite. *Earth and Planetary Science Letters*, 180(1-2), 133-148. [https://doi.org/10.1016/S0012-821X\(00\)00149-7](https://doi.org/10.1016/S0012-821X(00)00149-7)

Griffin, W. L., O'Reilly, S. Y., Afonso, J. C., & Begg, G. C. (2009). The Composition and Evolution of Lithospheric Mantle : A Re-evaluation and its Tectonic Implications. *Journal of Petrology*, 50(7), 1185-1204. <https://doi.org/10.1093/petrology/egn033>

Griffin, W. L., O'Reilly, S. Y., & Ryan, C. G. (1999). The composition and origin of sub-continental lithospheric mantle. In *Mantle Petrology : Field Observations and High Pressure Experimentation : A Tribute to Francis R. (Joe) Boyd (Vol. 6, p. 13-45)*. *Geochem. Soc. Spec. Publ.*

Gu, X., Deloule, E., France, L., & Ingrin, J. (2016). Multi-stage metasomatism revealed by trace element and Li isotope distributions in minerals of peridotite xenoliths from Allègre volcano (French Massif Central). *Lithos*, 264, 158-174. <https://doi.org/10.1016/j.lithos.2016.07.019>

Gu, X., Ingrin, J., Deloule, E., France, L., & Xia, Q. (2018). Metasomatism in the sub-continental lithospheric mantle beneath the south French Massif Central : Constraints from trace elements, Li and H in peridotite minerals. *Chemical Geology*, 478, 2-17. <https://doi.org/10.1016/j.chemgeo.2017.08.006>

Handler, M. R., Wysoczanski, R. J., & Gamble, J. A. (2003). Proterozoic lithosphere in Marie Byrd Land, West Antarctica : Re-Os systematics of spinel peridotite xenoliths. *Chemical Geology*, 196(1-4), 131-145. [https://doi.org/10.1016/S0009-2541\(02\)00410-2](https://doi.org/10.1016/S0009-2541(02)00410-2)

Hellebrand, E. (2002). Garnet-field Melting and Late-stage Refertilization in « Residual » Abyssal Peridotites from the Central Indian Ridge. *Journal of Petrology*, 43(12), 2305-2338. <https://doi.org/10.1093/petrology/43.12.2305>

Hellebrand, E., Snow, J. E., Dick, H. J. B., & Hofmann, A. W. (2001). Coupled major and trace elements as indicators of the extent of melting in mid-ocean-ridge peridotites. *Nature*, 410(6829), 677-681. <https://doi.org/10.1038/35070546>

Herzberg, C. (2011). Identification of Source Lithology in the Hawaiian and Canary Islands : Implications for Origins. *Journal of Petrology*, 52(1), 113-146. <https://doi.org/10.1093/petrology/egg075>

Herzberg, C. (2004). Geodynamic information in peridotite petrology. *Journal of Petrology*, 45(12), 2507-2530.

708 Hirose, K., & Kushiro, I. (1993). Partial melting of dry peridotites at high pressures : Determination of compositions of melts
 709 segregated from peridotite using aggregates of diamond. *Earth and Planetary Science Letters*, 114(4), 477-489.
 710 [https://doi.org/10.1016/0012-821X\(93\)90077-M](https://doi.org/10.1016/0012-821X(93)90077-M)

711 Hirschmann, M. M. (2000). Mantle solidus : Experimental constraints and the effects of peridotite composition: MANTLE
 712 SOLIDUS. *Geochemistry, Geophysics, Geosystems*, 1(10), n/a-n/a. <https://doi.org/10.1029/2000GC000070>

713 Hirschmann, M. M., Ghiorso, M. S., Wasylenki, L. E., Asimow, P. D., & Stolper, E. M. (1998). Calculation of Peridotite
 714 Partial Melting from Thermodynamic Models of Minerals and Melts. I. Review of Methods and Comparison with
 715 Experiments. *Journal of Petrology*, 39(6), 1091-1115. <https://doi.org/10.1093/petroj/39.6.1091>

716 Hofmann, A. W. (1997). Mantle geochemistry : The message from oceanic volcanism. *Nature*, 385(6613), 219-229.
 717 <https://doi.org/10.1038/385219a0>

718 Jakobsson, S. P., Jonsson, J., & Shido, F. (1978). Petrology of the Western Reykjanes Peninsula, Iceland. *Journal of*
 719 *Petrology*, 19(4), 669-705. <https://doi.org/10.1093/petrology/19.4.669>

720 Jollands, M. C., Hanger, B. J., Yaxley, G. M., Hermann, J., & Kilburn, M. R. (2018). Timescales between mantle
 721 metasomatism and kimberlite ascent indicated by diffusion profiles in garnet crystals from peridotite xenoliths. *Earth and*
 722 *Planetary Science Letters*, 481, 143-153.

723 Kelemen, Peter. B. (1990). Reaction Between Ultramafic Rock and Fractionating Basaltic Magma I. Phase Relations, the
 724 Origin of Calc-alkaline Magma Series, and the Formation of Discordant Dunite. *Journal of Petrology*, 31(1), 51-98.
 725 <https://doi.org/10.1093/petrology/31.1.51>

726 Kelemen, P.B., Dick, H.J., Quick, J.E., 1992. Formation of harzburgite by pervasivemelt/rock reaction in the upper mantle.
 727 *Nature* 358, 635–641.

728 Keller, T., & Katz, R. F. (2016). The role of volatiles in reactive melt transport in the asthenosphere. *Journal of Petrology*,
 729 57(6), 1073-1108.

730 Kornprobst, J. (1969). Le massif ultrabasique des Beni Bouchera (Rif Interne, Maroc) : Etude des péridotites de haute
 731 température et de haute pression, et des pyroxénolites, à grenat ou sans grenat, qui leur sont associées. *Contributions to*
 732 *Mineralogy and Petrology*, 23(4), 283-322. <https://doi.org/10.1007/BF00371425>

733 Kornprobst, J., Piboule, M., Roden, M., Tabit, A. (1990). Corundum-bearing garnet clinopyroxenites at Beni Bousera
 734 (Morocco): Original plagioclase-rich gabbros recrystallized at depth within the mantle? *Journal of Petrology*, 31(3), 717-
 735 745.

736 Kress, V. C., & Carmichael, I. S. (1988). Stoichiometry of the iron oxidation reaction in silicate melts. *American*
737 *Mineralogist*, 73(11-12), 1267-1274.

738 Lambart, S., Laporte, D., & Schiano, P. (2009). An experimental study of focused magma transport and basalt–peridotite
739 interactions beneath mid-ocean ridges : Implications for the generation of primitive MORB compositions. *Contributions to*
740 *Mineralogy and Petrology*, 157(4), 429-451. <https://doi.org/10.1007/s00410-008-0344-7>

741 Lambart, S., Laporte, D., Provost, A., & Schiano, P. (2012). Fate of Pyroxenite-derived Melts in the Peridotitic Mantle :
742 Thermodynamic and Experimental Constraints. *Journal of Petrology*, 53(3), 451-476.
743 <https://doi.org/10.1093/petrology/egr068>

744 Lambart, S., Laporte, D., & Schiano, P. (2013). Markers of the pyroxenite contribution in the major-element compositions of
745 oceanic basalts : Review of the experimental constraints. *Lithos*, 160-161, 14-36. <https://doi.org/10.1016/j.lithos.2012.11.018>

746 Lambart, S., Hamilton, S., & Lang, O. I. (2022). Compositional variability of San Carlos olivine. *Chemical Geology*, 605,
747 120968. <https://doi.org/10.1016/j.chemgeo.2022.120968>

748 Laumonier, M., Farla, R., Frost, D. J., Katsura, T., Marquardt, K., Bouvier, A.-S., & Baumgartner, L. P. (2017).
749 Experimental determination of melt interconnectivity and electrical conductivity in the upper mantle. *Earth and Planetary*
750 *Science Letters*, 463, 286-297. <https://doi.org/10.1016/j.epsl.2017.01.037>

751 Lawley, C. J. M., Pearson, D. G., Waterton, P., Zagorevski, A., Bédard, J. H., Jackson, S. E., Petts, D. C., Kjarsgaard, B. A.,
752 Zhang, S., & Wright, D. (2020). Element and isotopic signature of re-fertilized mantle peridotite as determined by
753 nanopowder and olivine LA-ICPMS analyses. *Chemical Geology*, 536, 119464.
754 <https://doi.org/10.1016/j.chemgeo.2020.119464>

755 Le Roux, V., Bodinier, J.-L., Alard, O., O'Reilly, S. Y., & Griffin, W. L. (2009). Isotopic decoupling during porous melt
756 flow : A case-study in the Lherz peridotite. *Earth and Planetary Science Letters*, 279(1-2), 76-85.
757 <https://doi.org/10.1016/j.epsl.2008.12.033>

758 Le Roux, V., Bodinier, J.-L., Tommasi, A., Alard, O., Dautria, J.-M., Vauchez, A., & Riches, A. J. V. (2007). The Lherz
759 spinel lherzolite : Refertilized rather than pristine mantle. *Earth and Planetary Science Letters*, 259(3-4), 599-612.
760 <https://doi.org/10.1016/j.epsl.2007.05.026>

761 Le Roux, V., Nielsen, S. G., Sun, C., & Yao, L. (2016). Dating layered websterite formation in the lithospheric mantle. *Earth*
762 *and Planetary Science Letters*, 454, 103-112. <https://doi.org/10.1016/j.epsl.2016.08.036>

763 Le Roux, V., Tommasi, A., & Vauchez, A. (2008). Feedback between melt percolation and deformation in an exhumed
764 lithosphere–asthenosphere boundary. *Earth and Planetary Science Letters*, 274(3-4), 401-413.
765 <https://doi.org/10.1016/j.epsl.2008.07.053>

766 Lorand, J.-P., & Luguët, A. (2016). Chalcophile and Siderophile Elements in Mantle Rocks : Trace Elements Controlled By
767 Trace Minerals. *Reviews in Mineralogy and Geochemistry*, 81(1), 441-488. <https://doi.org/10.2138/rmg.2016.81.08>

768 Mallik, A., & Dasgupta, R. (2013). Reactive Infiltration of MORB-Eclogite-Derived Carbonated Silicate Melt into Fertile
769 Peridotite at 3 GPa and Genesis of Alkalic Magmas. *Journal of Petrology*, 54(11), 2267-2300.
770 <https://doi.org/10.1093/petrology/egt047>

771 Mallmann, G., O'Neill, H. S. C., & Klemme, S. (2009). Heterogeneous distribution of phosphorus in olivine from otherwise
772 well-equilibrated spinel peridotite xenoliths and its implications for the mantle geochemistry of lithium. *Contributions to*
773 *Mineralogy and Petrology*, 158(4), 485-504.

774 McDonough, W. F., & Frey, F. A. (1989). Chapter 5. RARE EARTH ELEMENTS IN UPPER MANTLE ROCKS. In B. R.
775 Lipin & G. A. McKay (Éds.), *Geochemistry and Mineralogy of Rare Earth Elements* (p. 99-146). De Gruyter.
776 <https://doi.org/10.1515/9781501509032-008>

777 McKenzie, D., & Bickle, M. J. (1988). The Volume and Composition of Melt Generated by Extension of the Lithosphere.
778 *Journal of Petrology*, 29(3), 625-679. <https://doi.org/10.1093/petrology/29.3.625>

779 McKenzie, D., & O'Nions, R. K. (1991). Partial Melt Distributions from Inversion of Rare Earth Element Concentrations.
780 *Journal of Petrology*, 32(5), 1021-1091. <https://doi.org/10.1093/petrology/32.5.1021>

781 Menzies, M. A., & Dupuy, C. (1991). Orogenic Massifs : Protolith, Process and Provenance. *Journal of Petrology*,
782 *Special_Volume*(2), 1-16. https://doi.org/10.1093/petrology/Special_Volume.2.1

783 Mitchell, A. L., & Grove, T. L. (2016). Experiments on melt–rock reaction in the shallow mantle wedge. *Contributions to*
784 *Mineralogy and Petrology*, 171(12), 107. <https://doi.org/10.1007/s00410-016-1312-2>

785 Morgan, Z., & Liang, Y. (2003). An experimental and numerical study of the kinetics of harzburgite reactive dissolution
786 with applications to dunite dike formation. *Earth and Planetary Science Letters*, 214(1-2), 59-74.
787 [https://doi.org/10.1016/S0012-821X\(03\)00375-3](https://doi.org/10.1016/S0012-821X(03)00375-3)

788 Morgan, Z., & Liang, Y. (2005). An experimental study of the kinetics of lherzolite reactive dissolution with applications to
789 melt channel formation. *Contributions to Mineralogy and Petrology*, 150(4), 369-385. [https://doi.org/10.1007/s00410-005-](https://doi.org/10.1007/s00410-005-0033-8)
790 0033-8

791 Mundl, A., Ntaflou, T., Ackerman, L., Bizimis, M., Bjerg, E. A., Wegner, W., & Hauzenberger, C. A. (2016). Geochemical
792 and Os–Hf–Nd–Sr Isotopic Characterization of North Patagonian Mantle Xenoliths : Implications for Extensive Melt
793 Extraction and Percolation Processes. *Journal of Petrology*, 57(4), 685-715. <https://doi.org/10.1093/petrology/egv048>

794 Müntener, O., Pettke, T., Desmurs, L., Meier, M., & Schaltegger, U. (2004). Refertilization of mantle peridotite in
795 embryonic ocean basins : Trace element and Nd isotopic evidence and implications for crust–mantle relationships. *Earth and*
796 *Planetary Science Letters*, 221(1-4), 293-308. [https://doi.org/10.1016/S0012-821X\(04\)00073-1](https://doi.org/10.1016/S0012-821X(04)00073-1)

797 Müntener, O., & Piccardo, G. B. (2003). Melt migration in ophiolitic peridotites : The message from Alpine–Apennine
798 peridotites and implications for embryonic ocean basins. *Geological Society, London, Special Publications*, 218(1), 69-89.
799 <https://doi.org/10.1144/GSL.SP.2003.218.01.05>

800 Navon, O., & Stolper, E. (1987). Geochemical Consequences of Melt Percolation : The Upper Mantle as a Chromatographic
801 Column. *The Journal of Geology*, 95(3), 285-307. <https://doi.org/10.1086/629131>

802 Norman, M. D., & Garcia, M. O. (1999). Primitive magmas and source characteristics of the Hawaiian plume : Petrology and
803 geochemistry of shield picrites. *Earth and Planetary Science Letters*, 168(1-2), 27-44. [https://doi.org/10.1016/S0012-](https://doi.org/10.1016/S0012-821X(99)00043-6)
804 [821X\(99\)00043-6](https://doi.org/10.1016/S0012-821X(99)00043-6)

805 Niu, Y. (1997). Mantle Melting and Melt Extraction Processes beneath Ocean Ridges : Evidence from Abyssal Peridotites.
806 *Journal of Petrology*, 38(8), 1047-1074. <https://doi.org/10.1093/petroj/38.8.1047>

807 O’Driscoll, B., Walker, R. J., Day, J. M. D., Ash, R. D., & Daly, J. S. (2015). Generations of Melt Extraction, Melt–Rock
808 Interaction and High-Temperature Metasomatism Preserved in Peridotites of the ~497 Ma Leka Ophiolite Complex,
809 Norway. *Journal of Petrology*, 56(9), 1797-1828. <https://doi.org/10.1093/petrology/egv055>

810 Oliveira, B., Afonso, J. C., & Tilhac, R. (2020). A disequilibrium reactive transport model for mantle magmatism. *Journal of*
811 *Petrology*, 61(9), egaa067.

812 Pearson, D. G., Canil, D., & Shirey, S. B. (2014). Mantle Samples Included in Volcanic Rocks. In *Treatise on Geochemistry*
813 (p. 169-253). Elsevier. <https://doi.org/10.1016/B978-0-08-095975-7.00216-3>

814 Pec, M., Holtzman, B. K., Zimmerman, M., & Kohlstedt, D. L. (2015). Reaction infiltration instabilities in experiments on
815 partially molten mantle rocks. *Geology*, 43(7), 575-578.

816 Pilet, S., Baker, M. B., Müntener, O., & Stolper, E. M. (2011a). Monte Carlo Simulations of Metasomatic Enrichment in the
817 Lithosphere and Implications for the Source of Alkaline Basalts. *Journal of Petrology*, 52(7-8), 1415-1442.
818 <https://doi.org/10.1093/petrology/egr007>

819 Pilet, S., Baker, M. B., Müntener, O., & Stolper, E. M. (2011b). Monte Carlo Simulations of Metasomatic Enrichment in the
820 Lithosphere and Implications for the Source of Alkaline Basalts. *Journal of Petrology*, 52(7-8), 1415-1442.
821 <https://doi.org/10.1093/petrology/egr007>

822 Pilet, S., Baker, M. B., & Stolper, E. M. (2008). Metasomatized Lithosphere and the Origin of Alkaline Lavas. *Science*,
823 320(5878), 916-919. <https://doi.org/10.1126/science.1156563>

824 Pilet, S., Hernandez, J., Sylvester, P., & Poujol, M. (2005). The metasomatic alternative for ocean island basalt chemical
825 heterogeneity. *Earth and Planetary Science Letters*, 236(1-2), 148-166. <https://doi.org/10.1016/j.epsl.2005.05.004>

826 Raffone, N., Chazot, G., Pin, C., Vannucci, R., & Zanetti, A. (2009). Metasomatism in the Lithospheric Mantle beneath
827 Middle Atlas (Morocco) and the Origin of Fe- and Mg-rich Wehrlites. *Journal of Petrology*, 50(2), 197-249.
828 <https://doi.org/10.1093/petrology/egn069>

829 Rampone, E., Borghini, G., & Basch, V. (2020). Melt migration and melt-rock reaction in the Alpine-Apennine peridotites :
830 Insights on mantle dynamics in extending lithosphere. *Geoscience Frontiers*, 11(1), 151-166.
831 <https://doi.org/10.1016/j.gsf.2018.11.001>

832 Reisberg, L. (2021). Osmium isotope constraints on formation and refertilization of the non-cratonic continental mantle
833 lithosphere. *Chemical Geology*, 574, 120245. <https://doi.org/10.1016/j.chemgeo.2021.120245>

834 Rudnick, R. L., & Walker, R. J. (2009). Interpreting ages from Re–Os isotopes in peridotites. *Lithos*, 112, 1083-1095.
835 <https://doi.org/10.1016/j.lithos.2009.04.042>

836 Saal, A. E. (2001). Re-Os Isotopes in the Horoman Peridotite : Evidence for Refertilization? *Journal of Petrology*, 42(1),
837 25-37. <https://doi.org/10.1093/petrology/42.1.25>

838 Seyler, M., Lorand, J.-P., Dick, H. J. B., & Drouin, M. (2007). Pervasive melt percolation reactions in ultra-depleted
839 refractory harzburgites at the Mid-Atlantic Ridge, 15° 20'N : ODP Hole 1274A. *Contributions to Mineralogy and Petrology*,
840 153(3), 303-319. <https://doi.org/10.1007/s00410-006-0148-6>

841 Shaw, C. S. J., Lebert, B. S., & Woodland, A. B. (2018). Thermodynamic Modelling of Mantle–Melt Interaction Evidenced
842 by Veined Wehrlite Xenoliths from the Rockeskyllerkopf Volcanic Complex, West Eifel Volcanic Field, Germany. *Journal*
843 *of Petrology*, 59(1), 59-86. <https://doi.org/10.1093/petrology/egy018>

844 Simon, N. S. C., Carlson, R. W., Pearson, D. G., & Davies, G. R. (2007). The Origin and Evolution of the Kaapvaal Cratonic
845 Lithospheric Mantle. *Journal of Petrology*, 48(3), 589-625. <https://doi.org/10.1093/petrology/egl074>

846 Simon, N. S. C., Neumann, E.-R., Bonadiman, C., Coltorti, M., Delpech, G., Grégoire, M., & Widom, E. (2008). Ultra-
847 refractory Domains in the Oceanic Mantle Lithosphere Sampled as Mantle Xenoliths at Ocean Islands. *Journal of Petrology*,
848 49(6), 1223-1251. <https://doi.org/10.1093/petrology/egn023>

849 Smith, P. M., & Asimow, P. D. (2005). Adiatat_1ph : A new public front-end to the MELTS, pMELTS, and pHMELTS
850 models: ADIABAT_1PH FRONT-END. *Geochemistry, Geophysics, Geosystems*, 6(2).
851 <https://doi.org/10.1029/2004GC000816>

852 Sobolev, A. V., Hofmann, A. W., Sobolev, S. V., & Nikogosian, I. K. (2005). An olivine-free mantle source of Hawaiian
853 shield basalts. *Nature*, 434(7033), 590-597. <https://doi.org/10.1038/nature03411>

854 Song, Y., & Frey, F. A. (1989). Geochemistry of peridotite xenoliths in basalt from Hannuoba, Eastern China : Implications
855 for subcontinental mantle heterogeneity. *Geochimica et Cosmochimica Acta*, 53(1), 97-113. [https://doi.org/10.1016/0016-](https://doi.org/10.1016/0016-7037(89)90276-7)
856 [7037\(89\)90276-7](https://doi.org/10.1016/0016-7037(89)90276-7)

857 Soustelle, V., Tommasi, A., Bodinier, J. L., Garrido, C. J., & Vauchez, A. (2009). Deformation and Reactive Melt Transport
858 in the Mantle Lithosphere above a Large-scale Partial Melting Domain : The Ronda Peridotite Massif, Southern Spain.
859 *Journal of Petrology*, 50(7), 1235-1266. <https://doi.org/10.1093/petrology/egp032>

860 Soustelle, V., Walte, N. P., Manthilake, M. A. G. M., & Frost, D. J. (2014). Melt migration and melt-rock reactions in the
861 deforming Earth's upper mantle : Experiments at high pressure and temperature. *Geology*, 42(1), 83-86.
862 <https://doi.org/10.1130/G34889.1>

863 Stolper, E. (1980). A phase diagram for mid-ocean ridge basalts: preliminary results and implications for petrogenesis.
864 *Contributions to Mineralogy and Petrology*, 74(1), 13-27. doi:10.1007/BF00375485

865 Stracke, A., Hofmann, A. W., & Hart, S. R. (2005). FOZO, HIMU, and the rest of the mantle zoo : THE MANTLE ZOO.
866 *Geochemistry, Geophysics, Geosystems*, 6(5), n/a-n/a. <https://doi.org/10.1029/2004GC000824>

867 Tilhac, R., Morishita, T., Hanaue, N., Tamura, A., & Guotana, J. M. (2021). Systematic LREE enrichment of mantle
868 harzburgites: The petrogenesis of San Carlos xenoliths revisited. *Lithos*, 396, 106195.

869 Tilhac, R., Ceuleneer, G., Griffin, W. L., O'Reilly, S. Y., Pearson, N. J., Benoit, M., ... & Grégoire, M. (2016). Primitive arc
870 magmatism and delamination: petrology and geochemistry of pyroxenites from the Cabo Ortegal Complex, Spain. *Journal of*
871 *Petrology*, 57(10), 1921-1954.

872 Tomlinson, E. L., & Kamber, B. S. (2021). Depth-dependent peridotite-melt interaction and the origin of variable silica in
873 the cratonic mantle. *Nature Communications*, 12(1), 1082. <https://doi.org/10.1038/s41467-021-21343-9>

874 Turner, A. J., Katz, R. F., & Behn, M. D. (2015). Grain-size dynamics beneath mid-ocean ridges: Implications for
875 permeability and melt extraction. *Geochemistry, Geophysics, Geosystems*, 16(3), 925-946.

876 Van der Wal, D. V., & Bodinier, J.-L. (1996). Origin of the recrystallisation front in the Ronda peridotite by km-scale
877 pervasive porous melt flow. *Contributions to Mineralogy and Petrology*, 122(4), 387-405.
878 <https://doi.org/10.1007/s004100050135>

879 Waff, H. S., & Faul, U. H. (1992). Effects of crystalline anisotropy on fluid distribution in ultramafic partial melts. *Journal*
880 *of Geophysical Research*, 97(B6), 9003. <https://doi.org/10.1029/92JB00066>

881 Wang, C., Liang, Y., Dygert, N., & Xu, W. (2016). Formation of orthopyroxenite by reaction between peridotite and
882 hydrous basaltic melt: an experimental study. *Contributions to Mineralogy and Petrology*, 171(8), 1-18.

883 Warren, J. M. (2016). Global variations in abyssal peridotite compositions. *Lithos*, 248-251, 193-219.
884 <https://doi.org/10.1016/j.lithos.2015.12.023>

885 Watson, E. B., Brenan, J. M., Baker, D. R. (1990). "Distribution of fluids in the continental mantle." In *Continental mantle*,
886 Oxford Clarendon Press, pp. 111-125. 1990.

887 Wu, F.-Y., Walker, R. J., Yang, Y.-H., Yuan, H.-L., & Yang, J.-H. (2006). The chemical-temporal evolution of lithospheric
888 mantle underlying the North China Craton. *Geochimica et Cosmochimica Acta*, 70(19), 5013-5034.
889 <https://doi.org/10.1016/j.gca.2006.07.014>

890 Yaxley, G. M., & Green, D. H. (1998). Reactions between eclogite and peridotite : Mantle refertilisation by subduction of
891 oceanic crust. *Schweizerische mineralogische und petrographische Mitteilungen*, 78(2), 243-255.

892 Zhu, W., Gaetani, G. A., Fusseis, F., Montesi, L. G. J., & De Carlo, F. (2011). Microtomography of Partially Molten Rocks :
893 Three-Dimensional Melt Distribution in Mantle Peridotite. *Science*, 332(6025), 88-91.
894 <https://doi.org/10.1126/science.1202221>

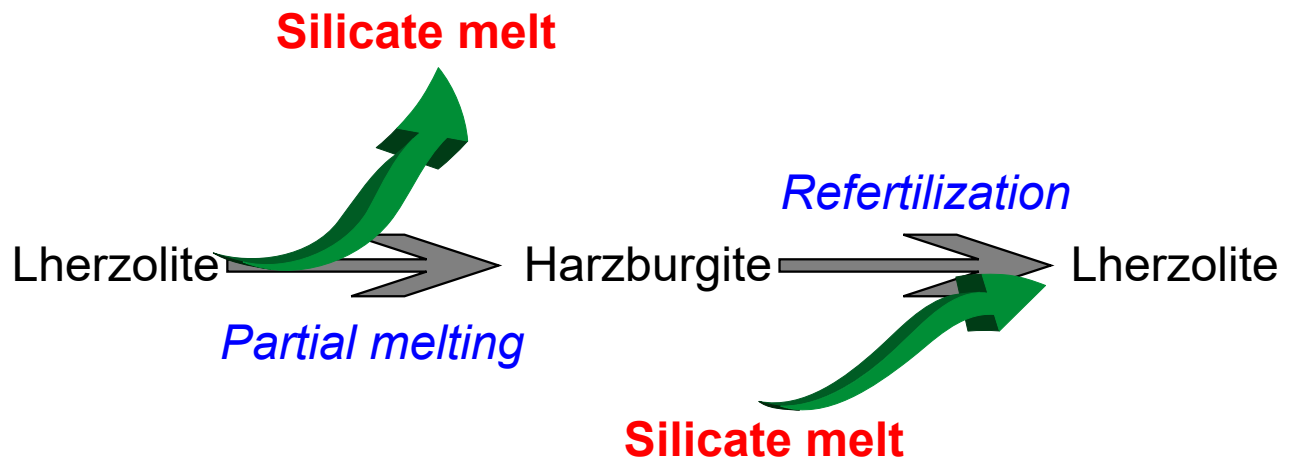
Fig 1. Schematization of the refertilization process in the context of lithospheric dynamics.

Fig 2. Evolution of modal mass proportions (in wt.%) of the different phases as a function of % of liquid added for run #1. a) Difference between modal proportion of each phase in the impregnated peridotite and its initial modal proportion in the starting material. For example, olivine represents 79.9 wt.% of the initial starting material but only 48.6 wt.% of the solid phase present at the end of the experiment, a change of -31.3. b) Absolute mass variation of each phase, for olivine, 79.9g of material are present at the beginning of the run, but only 72.9g at the end. (Ol: Olivine; Opx: Orthopyroxene; Cpx: Clinopyroxene; Sp: Spinel)

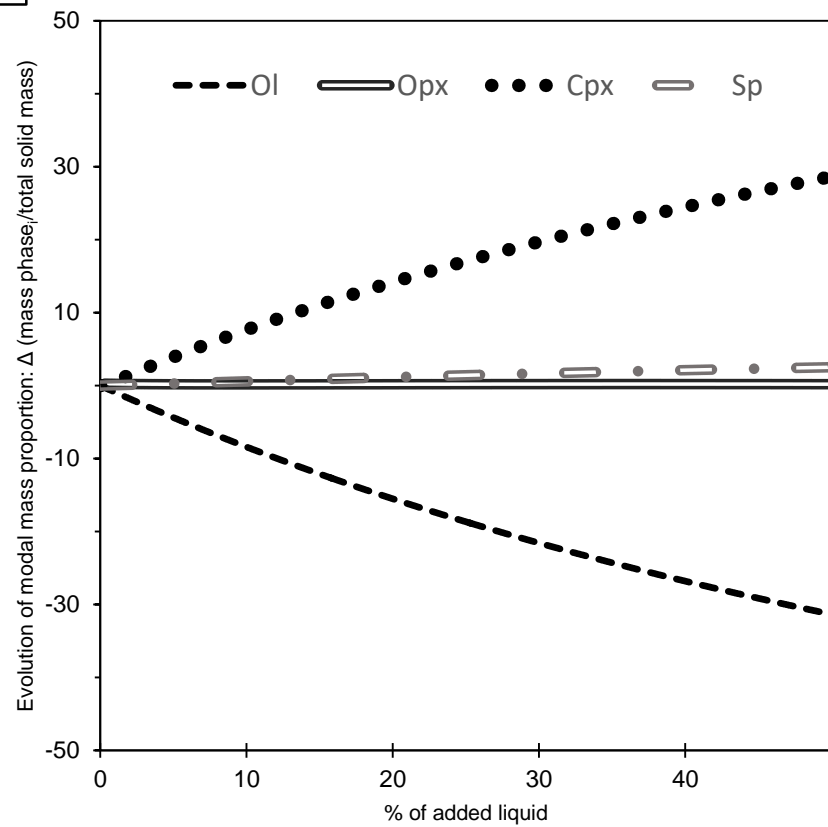
Fig 3. Evolution of modal proportions in models. Arrows indicate the direction of evolution of each run. In the impregnation calculations (runs #1 to #11), each tick mark indicates an addition of 10% of liquid. a) Runs #1 to #7b: influence of variations in pressure, temperature and redox conditions. b) Runs #1, #2, #10, and #11: influence of the chemical composition of the percolating melt c) Runs #1, #8, and #9: influence of the chemical composition of percolated harzburgite. d) Run #12: liquid-phase present run; run PM1: partial melting by isobaric rising temperature; run PM2: partial melting by decompression at constant T; run PM3: partial melting by isentropic decompression (constant S); and run #1: reference run. Partial melting runs by [Oliveira et al., 2020](#) are shown for comparison (DEM: Dynamic Equilibrium Melting; DFM: Dynamic Fractional Melting). Primitive upper mantle estimate is from [McDonough, 1995](#). Results are compared with modal proportions of a global database of tectonically emplaced peridotites ([Bodinier & Godard, 2014](#), and references therein).

Fig 4. Chemical diagrams displaying the variation of major element oxides (wt%) of the 6 runs comparing the influence of compositional variations (runs #1, #8, and #9: variation of the harzburgite composition; runs #1, #2, #10, and #11: variation of the percolating melt composition). Arrows indicate the direction of evolution of each test. Crosses on slopes are every 10% of liquid added. FeO_T: total iron content expressed as FeO. Results are compared with a global database of peridotites ([Bodinier & Godard, 2014](#), and references therein).

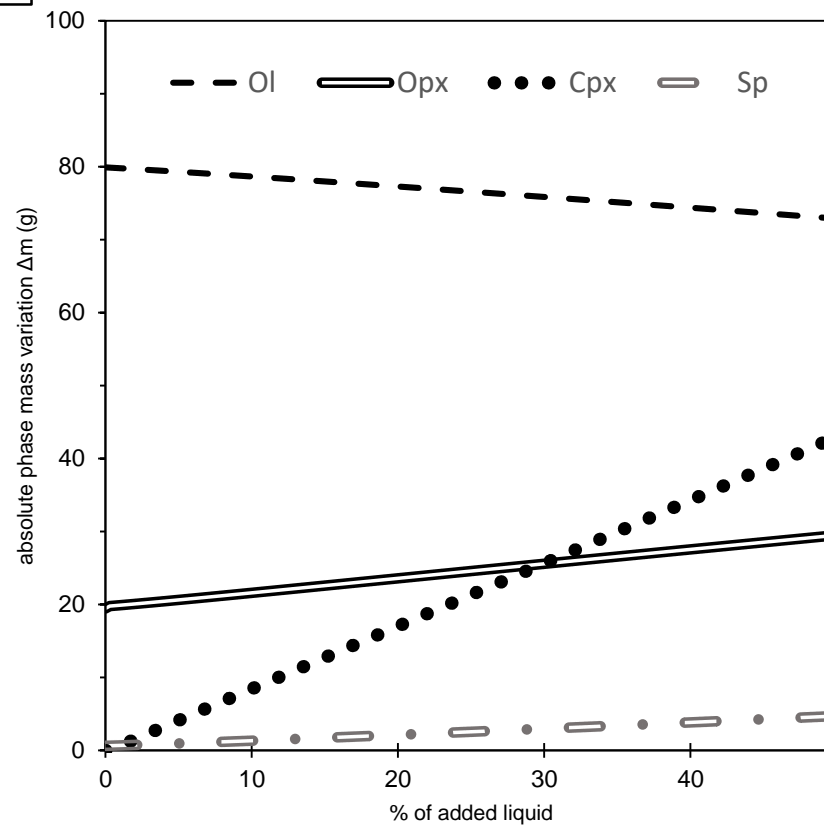
Fig 5. Variation of bulk major element concentrations (wt%) for the residual solid phase in runs #1, #12, PM1, PM2 and PM3. Run #12 is an impregnation run performed with a liquid phase present. Run PM1 is an isobaric partial melting run. Run PM2 is a partial melting run by decompression at constant T. Run PM3 is a partial melting run by isentropic decompression. Run #1 is shown for comparison. Arrows indicate the direction of evolution of each test. For runs #12 and #1, tick-marks on arrows indicate every 10% of liquid added. FeO_T: total iron content expressed as FeO. Results are compared with a global database of peridotites ([Bodinier & Godard, 2014](#), and references therein).



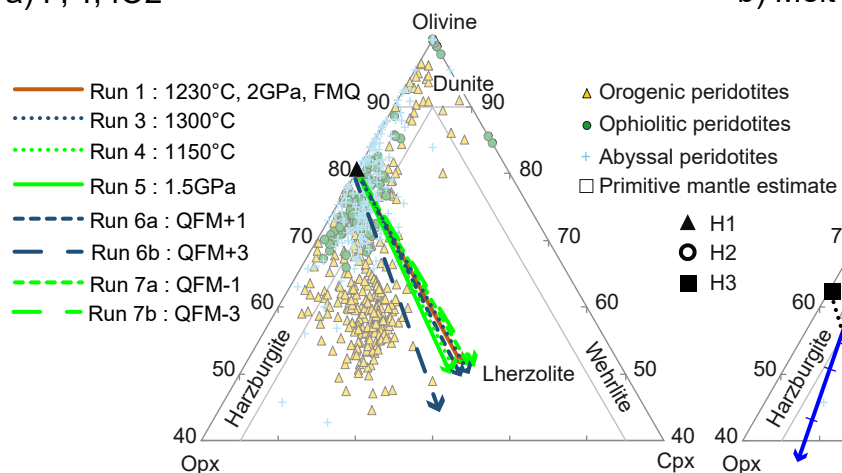
a)



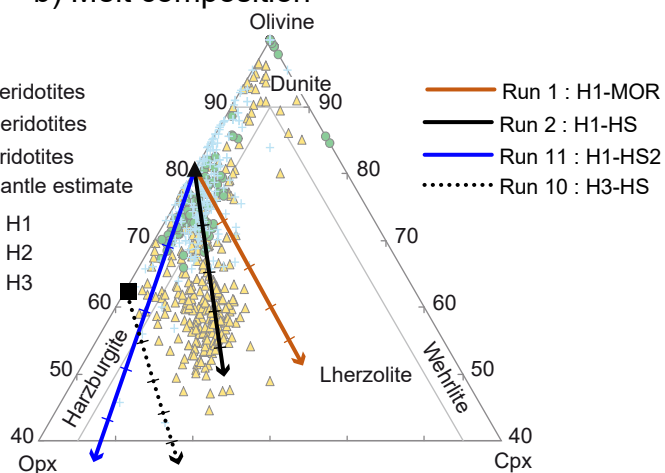
b)



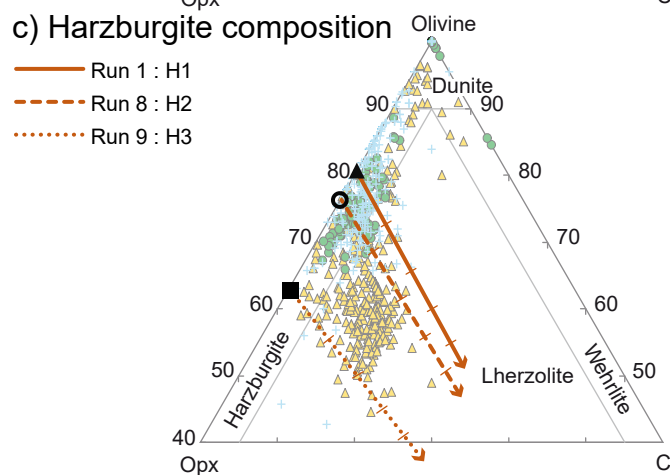
a) P, T, fO₂



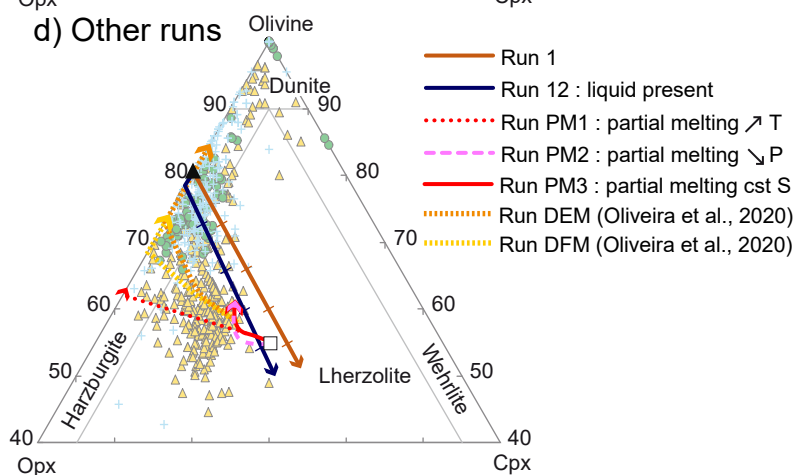
b) Melt composition

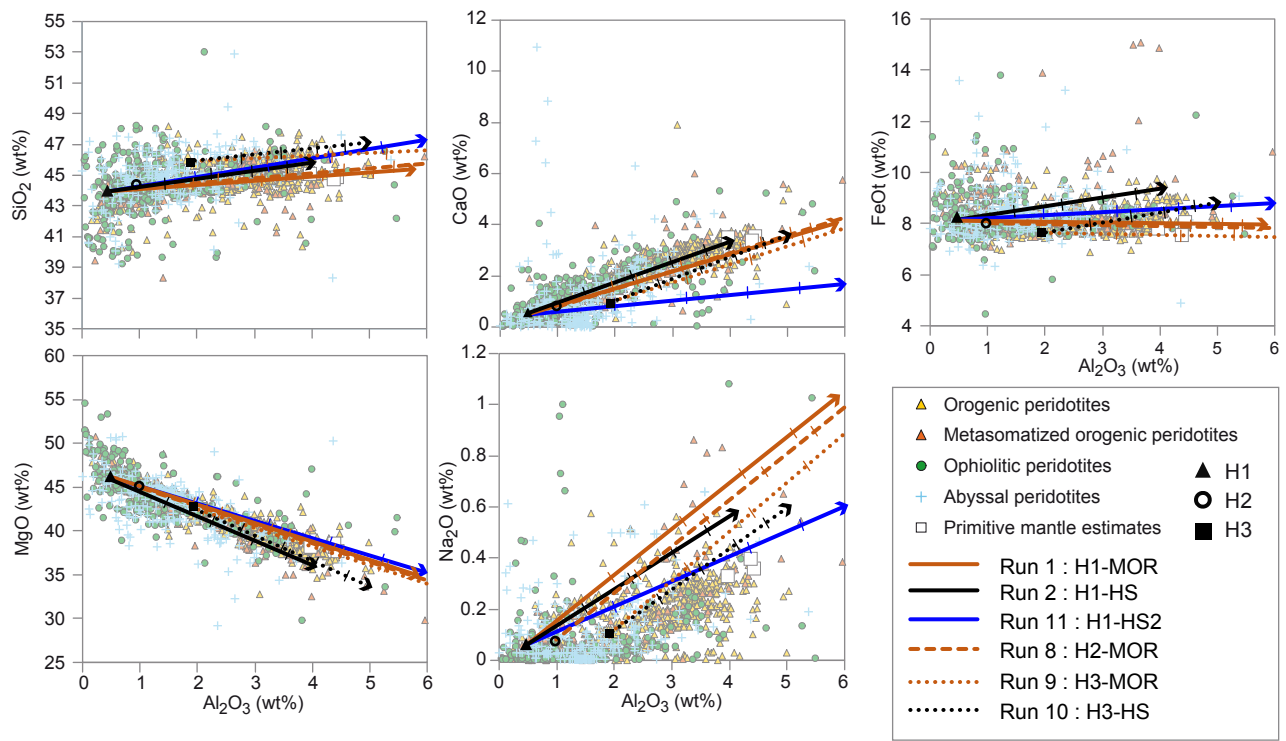


c) Harzburgite composition



d) Other runs





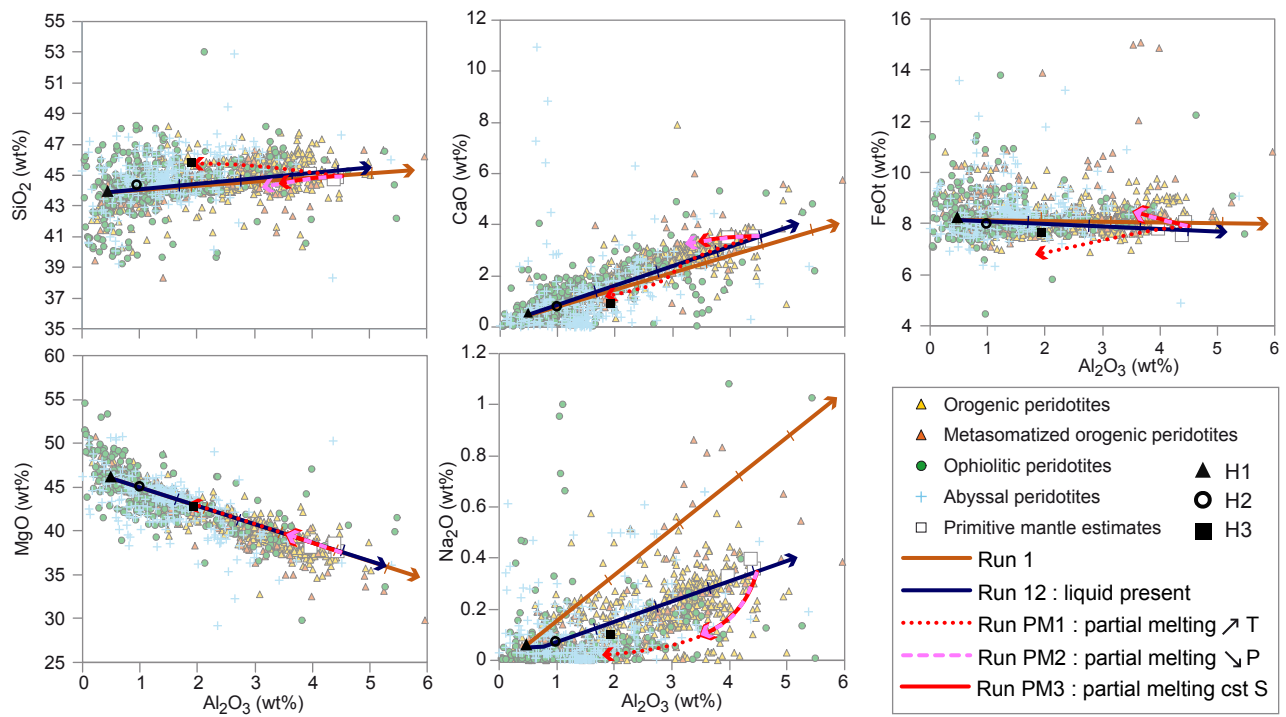


Table 1. Summary of thermodynamic parameters used in the calculations: temperature (*T*), pressure (*P*), oxygen fugacity (*fO*₂), starting composition and basaltic melt composition. (PM: Partial Melting; FMQ: Fayalite-Magnetite-Quartz oxygen buffer; H: Harzburgite; PUM: Primitive Upper Mantle; MOR: Mid-Ocean Ridge; HS: Hot Spot)

Run n°	T (°C)	P (GPa)	fO ₂	Starting composition	Melt composition
1	1230	2	FMQ	H1	MOR
2	1230	2	FMQ	H1	HS
3 ^a	1300	2	FMQ	H1	MOR
4	1150	2	FMQ	H1	MOR
5 ^a	1230	1.5	FMQ	H1	MOR
6a	1230	2	FMQ+1	H1	MOR
6b	1230	2	FMQ+3	H1	MOR
7a	1230	2	FMQ-1	H1	MOR
7b	1230	2	FMQ-3	H1	MOR
8	1230	2	FMQ	H2	MOR
9	1230	2	FMQ	H3	MOR
10	1230	2	FMQ	H3	HS
11	1230	2	FMQ	H1	HS2
12 ^a	1400	2	FMQ	H1	MOR
PM1	1200 - 1520	2	FMQ	PUM	-
PM2 ^b	1230	2 – 0.6	FMQ	PUM	-
PM3 ^c	1396 - 1213	2 – 0.6	FMQ	PUM	-

^a Liquid-present runs

^b Isothermal run

^c Isentropic run

Table 2. Chemical compositions of peridotites used in calculations.^a (H: Harzburgite; PUM: Primitive Upper Mantle)

	SiO ₂	Al ₂ O ₃	FeOt	MnO	MgO	CaO	Na ₂ O	Cr ₂ O ₃	TiO ₂
H1 ^b	43.91	0.47	8.19	0.13	46.57	0.38	0.05	0.31	0.01
H2 ^b	44.34	0.97	7.99	0.13	45.39	0.64	0.06	0.46	0.02
H3 ^b	45.82	1.92	7.49	0.13	42.95	0.75	0.09	0.82	0.04
PUM ^c	45.03	4.45	8.06	0.14	37.83	3.55	0.36	0.38	0.20

^a All compositions are normalized to 100 wt %. FeO_t: total iron content expressed as FeO.

^b Le Roux et al., 2007; ^c McDonough, 1995.

Table 3. Chemical compositions of percolating basaltic melts used in calculations.^a (MOR: Mid-Ocean Ridge; HS: Hot Spot)

	SiO ₂	Al ₂ O ₃	FeOt	MnO	MgO	CaO	Na ₂ O	Cr ₂ O ₃	TiO ₂	a _{SiO2} b
MOR^c	48.76	16.65	7.20	0.14	11.48	11.75	3.03	0.12	0.87	0.372
HS^d	50.01	11.37	11.48	0.18	13.98	9.26	1.66	0.00	2.06	0.485
HS2^e	54.32	17.18	9.93	0.18	11.98	3.87	1.73	0.12	0.69	0.551

^a All compositions are normalized to 100 wt %. FeOt: total iron content expressed as FeO.

^b Silica activities were calculated using the MELTS supplemental calculator.

^c Lambart et al., 2009; ^d Norman & Garcia, 1999; ^e Jakobsson, 1978.

Table 4. Final phases proportions for all runs (in wt.%). (PM: Partial Melting)

Run n°	Liquid	Olivine	Orthopyroxene	Clinopyroxene	Spinel
1	0.0	48.6	19.7	28.6	3.1
2	0.0	48.7	30.2	19.5	1.5
3	0.9	47.6	19.4	28.9	3.1
4	0.0	48.6	21.2	27.0	3.3
5	1.6	47.3	21.7	26.2	3.3
6a	0.0	47.5	20.8	28.4	3.3
6b	0.0	42.5	25.8	27.4	4.4
7a	0.0	49.2	19.0	28.8	3.1
7b	0.0	49.7	18.4	28.9	3.0
8	0.0	44.7	22.3	29.3	3.7
9	0.0	35.0	31.3	29.0	4.6
10	0.0	34.6	42.4	19.8	3.1
11	0.0	35.1	52.5	8.5	3.9
12^a	7.5	44.0	21.8	23.8	3.0
PM1	29.8	43.8	25.2	0.0	1.2
PM2^b	7.5	56.2	20.9	12.7	2.8
PM3^c	4.9	57.7	21.6	13.0	2.7

^a Liquid-present run

^b Isothermal run

^c Isentropic run

Silicate melt

Lherzolite

Partial melting

Harzburgite

Refertilization

Lherzolite

Silicate melt

Thermodynamic MELTS model
of melt addition to harzburgite
→ *Model refertilization process*

